CYCLOSTATIONARITY BASED BLIND CLASSIFICATION AND PARAMETER ESTIMATION FOR FSK AND MSK SIGNALS

HONGFEI WANG

Cyclostationarity based blind classification and parameter estimation for FSK and MSK signals

by

©Hongfei Wang

A Thesis submitted to the School of Graduate Studies in partial fulfillment of the requirements for the degree of

Master of Engineering

Faculty of Engineering and Applied Science

Memorial University of Newfoundland

September 2012

St. John's Newfoundland

Abstract

Blind signal classification and parameter estimation plays an important role in both military and civilian applications. The classification and estimation task provides signal information, such as modulation type, carrier frequency, signal bandwidth, and symbol timing, for the design of effective communication systems. In general, blind signal classification and parameter estimation is very challenging, particularly in environments involving a low signal-to-noise ratio (SNR) regime, short observation periods, fading channel conditions and relaxed a priori information.

Due to its easy implementation and widespread usage in legacy communications equipment, the frequency shift keying (FSK) modulation continues to be very common, especially in the VHF and UHF bands. On the other hand, minimum shift-keying (MSK) scheme is also widely used in wireless communication systems as it possesses many advantages, such as bandwidth efficiency and constant-envelope property. Thus, the blind classification and parameter estimation of FSK and MSK signals becomes an attractive research area. Most of existing approaches for FSK and MSK signal classification and parameter estimation require pre-processing such as symbol timing and carrier recovery, and only additive Gaussian noise (AWGN) channel is considered.

In this thesis, the cyclostationarity-based FSK and MSK signal classification and parameter estimation are studied. The first- and second-order cyclostationarity of

FSK and MSK signals affected by fading is investigated. Based on the first-order cyclostationarity of FSK signals, a joint classification and tone frequency spacing estimation algorithm is proposed. Furthermore, a symbol period estimation algorithm for FSK signals is proposed based on the properties of second-order cyclostationarity. By combining the properties of first- and second-order cyclostationarity of FSK and MSK signals, a joint classification algorithm for FSK and MSK signals is proposed. Simulation and experimental results are carried out to show the efficiency of proposed algorithms. It is proved that reasonably good performance can be obtained at low SNRs, using short observation period, under the fading effect, and with relaxed *a priori* information.

Acknowledgements

I would like to thank my supervisors Dr. Octavia A. Dobre and Dr. Cheng Li, for their support, suggestions, and encouragement throughout my master's program. They educated me with their abundant engineering knowledge and guided me patiently all the time. Without their persistent help, this thesis would not have been possible.

My sincere thanks also go to Dr. Venkatesan and Dr. Yuanzhu Peter Chen. I greatly appreciate their support and guidance when I was working on graduate courses and conducting research related to wireless sensor network.

I am grateful to the generous financial support from the Defence Research and Development Canada (DRDC) and the great opportunity being a research assistant under the contract with DRDC and Memorial University of Newfoundland.

I always remember the help and guidance from Mr. Nolan White in the Department of Computer Science, who offered me the computational facilities for my simulations. His help made it possible for me to obtain results running numerous simulation trials.

I also appreciate for Dr. Weimin Huang's help during my life in Memorial University. His suggestion and encouragement provided me with inspiration and confidence in my research work.

I would also like to thank the members of the Computer Engineering Research

laboratories (CERL), which provided a friendly and resourceful environment for conduct my research. Thanks especially to Walid A. Jerjawi, who helped me to solve many problems with the signal generator and analyzer facilities.

There are too many friends to mention individually, who have assisted me in so many ways during my study and life. I would like to thank Ruoyu Su, Yi Zhang, Zehua Wang, Jie Chen, Walid A. Jerjawi, Yahia A. Eldemerdash, and Ebrahim Bedeer for the help during my research work. I would also like to thank Dr. Shuai Han and his family, Cheng Wang, Shuang Wu, Jianhui Feng, Yan Luo, and many friends whose names are not mentioned.

Last, and most important, I would like to thank my family. I cannot find words to express my gratitude to my dear girlfriend Fan Zhang for all her love and encouragement. I also owe a lot to my parents for their continuous support and endless love. I dedicate my thesis to them.

Table of Contents

List of Tables

List of Figures

List of Abbreviations

ADC	Analog-to-digital converter
AM	Amplitude modulation
ARB	Arbitrary waveform generator
AWGN	Additive white Gaussian noise
CF	Cycle frequency
CM	Cyclic moment
CPFSK	Continuous phase frequency shift keying
CPM	Continuous Phase Modulation
CR	Cognitive radio
DAC	Digital-to-analog converter
FB	Feature based
FCC	Federal communication commission
i.i.d.	Independent and identically distributed
IMR	Integer multiple relationship
LB	Likelihood based
MSK	Minimum shift keying
OFDM	Orthogonal frequency division multiplexing
PC	Personal computer
PSD	Power spectrum density

PSK	Phase shift keying
QAM	Quadrature amplitude modulation
SC	Selection combining
SDR	Software defined radio
SNR	Signa-to-noise ratio
UHF	Ultra high frequency
VHF	Very high frequency
VSA	Vector signal analyzer
VSG	Vector signal generator
WT	Wavelet transform

Chapter 1

Introduction

1.1 Blind signal classification and parameter estimation

The research on blind signal classification and parameter estimation investigates the processing of received signals for the purpose of extracting required information without or with very limited knowledge of the original signal. Research on the signal classification problems mainly focuses on identifying the signal modulation types, whereas the estimation problems study how to estimate the value of parameters that can not observed directly. It is of practical importance in wireless communication that classification and estimation task be completed based on limited prior information of received signals. Applications of blind signal classification and parameter estimation are found in many areas, such as electronic surveillance, interference identification, suitable jamming signal selection, and spectrum monitoring [1]- [2].

In wireless communications, blind signal classification and parameter estimation can be used to obtain basic signal information such as modulation type and symbol timing so as to facilitate the effective design of receivers. Moreover, blind classification

and estimation task can also improve the transmission efficiency by reducing the data overhead and training sequence. These advantages make blind signal classification and parameter estimation very attractive for software defined radio (SDR) application [3]. In the SDR system, the hardware is controlled by internal software so that it is able to adjust its parameters according to the radio environment and support various processing functions. It is highly desirable that the receiver can perform its functions by extracting the appropriate information from the received signal, e.g. modulation type, coding rate, channel bandwidth, and antenna configuration.

Another important application for blind signal classification and parameter estimation is in cognitive radio (CR) [4]. Recently, the progressively increasing demand for radio communications services has aggravated the problem of spectrum scarcity. The observation that many of the licensed spectrum bands are, on average, underutilized [5] has led to the notion of the CR as a way of resolving the spectrum scarcity problem. The key idea is to allow CR users access unutilized channels (spectral whitespace) allocated to the primary (incumbent) users, if they do not cause harmful interference. The ability of a CR to dynamically adapt to the radio environment is critically dependent on spectrum sensing and awareness [4]. These functions involve signal detection, classification, and parameter estimation. By classifying the modulation type or estimating important parameters of the transmitted signals of primary users, CR users are able to obtain the knowledge of spectrum occupation.

Blind signal classification and parameter estimation has been extensively studied on various types of modulation schemes. The vast majority of research focus on single carrier linear modulations such as phase shift keying (PSK) [6] and quadrature amplitude modulation (QAM) [7], orthogonal frequency division multiplexing (OFDM) [8]- [9], and frequency shift keying (FSK) [10]- [21]. Various approaches have been developed to extract the important signal parameters such as modulation

order, symbol timing, carrier frequency, signal bandwidth, etc. In general, blind signal classification and parameter estimation is very challenging, particularly in environments involving a low signal-to-noise ratio (SNR) regime, short observation periods, fading channel conditions and relaxed *a priori* information.

In this thesis, we focus on the blind signal classification and parameter estimation of FSK and MSK signals. Although classification of FSK signals are extensively studied, most of work only considered the additive Gaussian white noise (AWGN) channel condition. Moreover, very little work has been carried out on FSK signal parameter estimation and MSK signal classification. Thus, it is our goal to develop classification and parameter estimation algorithms for FSK and MSK signals in fading channels which does not require prior knowledge of received signals.

1.2 FSK signal classification

Due to its easy implementation and widespread usage in legacy communications systems, the frequency shift keying (FSK) modulation continues to be a common choice for communication equipments, especially in the very high frequency (VHF) and ultra high frequency (UHF) bands. Considerable research work has been conducted to explore the FSK signal classification, which can be grouped into two broad categories, likelihood-based (LB) and feature-based (FB) methods. The LB approach is based on the likelihood function of the received signal using a likelihood ratio test for the classification decision, whereas the FB approach utilizes the existence of the extracted features of received signals to identify the modulation type.

The LB approach is investigated in [10]- [11], in which a higher-order correlation FB algorithm is also jointly considered with the LB method. Signal parameter information such as symbol rate, tone frequency spacing, and signal and noise powers, is

required. A wavelet transform (WT) FB method is proposed in [12]. This requires symbol timing recovery to achieve an acceptable classification performance at lower SNRs. An FB method based on the mean of the complex signal envelope is presented in [13], however, symbol timing recovery is also required. A Fourier transform is employed in [14] to classify FSK signals. First-order cyclostationarity was utilized for amplitude modulation (AM) and FSK signal detection and classification in [15]-[17]. In [18], FSK signals are identified based on the zero-crossing sequence. Another algorithm that classifies FSK signals versus other signal classes, such as PSK, is studied in [19] by employing the information provided by the instantaneous frequency. However, carrier recovery is required for the algorithm to function.

Channel effects may have big impact on signal classification and parameter estimation, particularly in terrestrial environments. An additive white Gaussian noise (AWGN) channel is considered in [10]- [19]. Classification of FSK signals in Rayleigh fading channels is studied in [20] based on the LB approach, by assuming known symbol timing. When the timing information is unknown, the likelihood function is averaged over the timing offset, which inevitably increases the computational complexity. In addition, the symbol period still needs to be known, and the performance is sensitive to a carrier frequency offset. An instantaneous frequency FB method is proposed when the FSK signals are affected by fading [21]; however, it requires the knowledge of the tone frequency spacing and symbol period.

1.3 FSK signal parameter estimation

For FSK signals, tone frequency spacing and symbol period are two important parameters for further processing. In the previous studies, not much work has been conducted on tone frequency spacing estimation. A Fourier transform based method

is proposed in [14], where the tone frequency spacing is calculated according to the distance between spectrum peaks.

On the other hand, WT-based methods for FSK signal symbol period estimation have been studied in [22]- [24]. By utilizing WT to locate the transients produced from frequency changes and the separation between transients, symbol period can be estimated.

In [22], the WT magnitude is autocorrelated to reduce the noise and exploit the periodicity so that the peaks from transients become apparent. The separation of peaks provides the possibility of symbol period estimation. This algorithm is improved in [23] by taking the Fourier transform of WT magnitude before estimation. After applying the Fourier transform, significant peaks are obtained in the spectrum which provides a more accuracy estimate of symbol period. In [24], the carrier frequency of received signal is moved to zero before WT and therefore obtains a better estimation performance. However, prior knowledge of carrier frequency is required.

1.4 Joint classification of FSK and MSK signals

Continuous Phase Modulation (CPM) systems have generated great interest due to their bandwidth efficiency and constant-envelope property [26]- [27]. As an important form of CPM, minimum shift-keying (MSK) scheme is widely used in wireless communication systems. Thus, algorithms which can effectively identify MSK signals are required in various applications [28]- [31].

In [28], a decision-theoretic approach is proposed to classify different digitally modulated signals including MSK signals. A set of key features are considered at the classifier, such as the standard deviation of the normalized instantaneous frequency and the maximum value of the power spectral density (PSD) of the normalized in-

stantaneous frequency. Since MSK signals have less frequency components than FSK signals, the PSD of instantaneous frequency for MSK signals is less than that of FSK signals. This feature can be utilized to distinguish MSK and FSK signals. Another method is proposed in [29], which utilizes the instantaneous amplitude to separate FSK and MSK signals from linearly modulated signals. By examining the peaks in the spectrum, MSK and FSK signals can be distinguished. The algorithm proposed in [30] calculates the spectral correlation of the received signals for MSK signal classification based on the position of spectral peaks.

1.5 Thesis objective

The drawbacks of the previously proposed work for FSK and MSK signal classification and parameter estimation make it necessary to develop more efficient algorithms which are able to achieve a reasonable performance at low SNRs, using short observation periods, under the fading channel conditions, and with relaxed *a priori* information.

The first objective of this thesis is to investigate the cyclostationarity of FSK and MSK signals. We study the first-order cyclostationarity of FSK and MSK signals in particular, under the fading channel conditions, and we extend the study to second-order cyclostationarity. To the best of our knowledge, there is not such work carried out for the study of second-order cyclostationary properties of FSK and MSK signals.

The second objective of this thesis is to develop blind classification and parameter estimation algorithms for FSK and MSK signals based on their cyclostationary properties. The proposed algorithms do not require pre-processing such as timing and carrier recovery. The first-order cyclostationary properties of FSK signals are used for FSK signal classification and tone frequency spacing estimation. Classification and estimation tasks are carried out jointly. Besides tone frequency spacing, symbol pe-

riod is also an important parameter for FSK signals. Therefore, we further explore the second-order cyclostationary properties of FSK signals for symbol period estimation. By combining the first- and second-order cyclostationarity of FSK and MSK signals, a joint FSK and MSK classification algorithm is proposed. The performance of the proposed algorithms are evaluated using extensive simulations and experimental tests.

1.6 Thesis organization

The rest of the thesis is organized as follows.

In Chapter 2, the signal model and cyclostationarity of received FSK and MSK signals are introduced. The FSK signal model affected by fading channels and additive Gaussian white noise is presented. Based on the proposed signal model, the first- and second-order cyclostationarity of received FSK signals are obtained, including time-varying moment, cyclic moment, and cycle frequencies. The model of the received MSK signal is then presented, and findings on its first- and second-order cyclostationarity are also given.

In Chapter 3, algorithms for FSK and MSK signal classification and FSK signal parameter estimation are proposed. Based on the properties of first-order cyclostationarity of FSK signals, FSK signal classification and tone frequency estimation algorithm is proposed. The modulation order of FSK signals can be determined based on the number of detected cycle frequencies (CFs), and the tone frequency spacing can be calculated according to the position of CFs. Then, the properties of second-order cyclostationarity of FSK signals are developed. The absolute value of the second-order cyclic moment at zero CF has a series of spectrum peaks, and the peak pattern changes when the delay equals the symbol period. Based on this property, the FSK signal symbol period estimation algorithm is proposed. Furthermore, by combining

the first- and second-order cyclostationary properties of FSK and MSK signals, a joint FSK and MSK classification algorithms is proposed.

In Chapter 4, Monte Carlo simulations are conducted to evaluate the performance of each proposed algorithm. Simulation results show that the proposed algorithms provide reasonably good performance even under short observation period, low SNRs, and in fading channel conditions. The performance can be further improved by exploring the spatial diversity at the receiver side. Moreover, experimental results are also given for FSK and MSK signal classification and FSK tone frequency estimation. As expected, the experimental results match well with those obtained through simulations.

Finally, the conclusions and suggestions for future work are provided in Chapter 5.

1.7 Major contributions of the thesis

The major contributions presented in each chapter are:

- Chapter 2: Analytical expressions of first- and second-order cyclostationarity for FSK and MSK signals affected by fading.
- Chapter 3: (1) First-order cyclostationarity based FSK signal classification and tone frequency spacing estimation algorithm. (2) Second-order cyclostationarity based FSK signal symbol period estimation algorithm. (3) Joint FSK and MSK signal classification algorithm.
- Chapter 4: Performance evaluations of the proposed algorithms through computer simulations. Evaluation of FSK and MSK classification performance and FSK signal tone frequency spacing using laboratory experiments.

This thesis work has led to the following research publications:

Full paper refereed conference publications: accepted/published

- H. Wang, O. A. Dobre, C. Li, and R. Inkol, "M-FSK signal recognition in fading channels for cognitive radio," in *Proc. IEEE Radio and Wireless Symposium*, Jan. 2012.

- H. Wang, O. A. Dobre, C. Li, and R. Inkol, "Joint classification and parameter estimation of M-FSK signals for cognitive radio," in *Proc. IEEE International Conference on Communications*, Jun. 2012.

Full paper refereed journal/conference publications: submitted/under preparation

- H. Wang, O. A. Dobre, C. Li, and R. Inkol, "Experimental results for joint FSK signal classification and parameter estimation algorithm," submitted to *IEEE I2MTC*, 2013.

- H. Wang, O. A. Dobre, C. Li, and R. Inkol, "Second-order cyclostationarity based symbol period estimation of FSK signals for cognitive radio," will submit to *IEEE Communication Letters*, 2012.

- H. Wang, O. A. Dobre, C. Li, and R. Inkol, "A novel cyclostationarity based classification algorithm for FSK and MSK signals," will submit to *IEEE Trans. Instrum. and Meas.*, 2012.

Chapter 2

Signal models and corresponding cyclostationarity

2.1 Introduction

In this chapter, we investigate FSK and MSK signals. The former is mainly used in VHF and UHF bands, and its advantages such as ease of implementation and abundant legacy of equipments make it still common used in various applications. The latter is a continuous phase frequency shift keying signal, which is bandwidth and energy efficient. In the following section, we first present the model of FSK signals, and then study their first- and second-order cyclostationarity. Then we present the model of MSK signals, their first- and second-order cyclostationarity. The cyclostationary properties of FSK and MSK signals will be further exploited in Chapter 3, where we propose signal classification and parameter estimation algorithms.

2.2 FSK signal model and its cyclostationarity

2.2.1 FSK signal model

The received signal affected by block fading and additive Gaussian noise can be expressed as

$$r_{FSK}(t) = ae^{j\phi}e^{j2\pi\Delta f_c t}\sum_i e^{j2\pi s_i f_d(t-iT)}u_T(t-iT) + w(t), \tag{2.1}$$

where a and ϕ represent the amplitude and phase introduced by the channel, respectively, Δf_c is the frequency offset, s_i is the data symbol transmitted during the ith period, which takes values from the alphabet $A_\Omega = \{\pm 1, \pm 3, ... \pm (\Omega - 1)\}$, with equal probability and Ω denotes the modulation order, f_d equals half of the tone frequency spacing, T is the symbol period, $u_T(t)$ is the signal pulse shape function, which equals 1 over the symbol period and zero otherwise, and $w(t)$ is the zero-mean additive Gaussian noise. Following proofs are based on the assumption that $l = f_d T$, l integer.

2.2.2 First-order cyclostationarity of FSK signal

Given the first-order cyclostationarity of the signal $r(t)$, its first-order moment $\hat{m}_r(t) = E\{r(t)\}$ is an (almost) periodic function of n, which can be expressed as a Fourier series [32],

$$\hat{m}_r(t) = \sum_{\alpha\in\kappa} M_r(\alpha)e^{j2\pi\alpha l}. \tag{2.2}$$

Here $E\{.\}$ denotes the expectation operator, $M_r(\alpha)$ is the first-order cyclic moment (CM) at the cycle frequency (CF) α, and $\kappa = \{\alpha : M_r(\alpha) \neq 0\}$ represents the set of first-order CFs. The first order CM is defined as

$$M_r(\alpha) = \lim_{I\to\infty} I^{-1}\int_{-I/2}^{I/2} \hat{m}_r(t)e^{-j2\pi\alpha l}dt. \tag{2.3}$$

By following the approach presented in [17], the first-order CM of the FSK signals affected by block fading can be obtained as

$$M_{r_{FSK}}(\alpha) = \Omega^{-1} a e^{j\phi}, \tag{2.4}$$

with the CFs belonging to the set

$$\kappa = \{\alpha : \alpha = qT^{-1}f_s^{-1} + \Delta f_c f_s^{-1}, q = \pm l, ..., \pm(\Omega - 1)l,\ l = f_d T,\ l\ integer\}. \tag{2.5}$$

Note that the first-order CM is zero at frequencies other than the CFs. From the above equation, we further note that the number of first-order CFs is equal to two, four, and eight, for 2-FSK, 4-FSK, and 8-FSK signals, respectively.

2.2.3 Second-order cyclostationarity of FSK signal

For a cyclostationary process $r(t)$, the second-order time-varying moment is given by [32].

$$m_r(t, \tau) = E\{r(t)r^*(t - \tau)\}. \tag{2.6}$$

Here, τ is the time delay and * represents the conjugate operation. As $r(t)$ is a cyclostationary process, $m_r(t, \tau)_{2,1}$ accepts a Fourier series with respect to time t, as [32]

$$m_r(t, \tau) = \sum_{\beta \epsilon \kappa} M_r(\beta, \tau) e^{j2\pi\beta t}, \tag{2.7}$$

where the Fourier coefficient $M_r(\beta, \tau)$ is the second-order CM at cycle frequency (CF) β, and $\kappa = \{\beta : M_r(\beta, \tau) \neq 0\}$ represents the set of second-order CFs. For the received

FSK signal[1], the second-order time-varying moment, CM, and set of CFs are given in (2.8), (2.9), and (2.10), respectively. The proof is subsequently provided.

$$m_{r_{FSK}}(t,\tau) = \begin{cases} \frac{a^2 e^{j2\pi\Delta f_c \tau}}{\Omega} \sum_i \sum_{n=1}^{\Omega} e^{j2\pi \tilde{s}_n f_d \tau_0} (u_T(t-iT) \\ \times u_T(t-iT-\tau_0) + \frac{1}{\Omega} \sum_{m+1}^{\Omega} e^{j2\pi(\tilde{s}_m - \tilde{s}_n) f_d (t-iT)} \\ \times u_T(t-iT) u_T(t-(i-\mu)T-\tau_0)), & |\tau| < T, \\ \\ \frac{a^2 e^{j2\pi\Delta f_c \tau}}{\Omega^2} \sum_i \sum_{m=1}^{\Omega} \sum_{n=1}^{\Omega} e^{j2\pi(\tilde{s}_m - \tilde{s}_n) f_d (t-iT)} \\ \times e^{j2\pi \tilde{s}_n f_d \tau_0} (u_T(t-iT) u_T(t-iT-\tau_0) \\ + u_T(t-iT) u_T(t-(i-\mu)T-\tau_0)), & |\tau| \geq T, \end{cases} \tag{2.8}$$

$$M_{r_{FSK}}(\alpha,\tau) = \begin{cases} \frac{a^2 e^{j2\pi\Delta f_c \tau}}{T\Omega} \sum_{n=1}^{\Omega} e^{j2\pi \tilde{s}_n f_d \tau_0} (U_1(\alpha) + \frac{1}{\Omega} \sum_{m=1}^{\Omega} \\ \times U_2(\alpha - (\tilde{s}_m - \tilde{s}_n) f_d)), & |\tau| < T, \\ \\ \frac{a^2 e^{j2\pi\Delta f_c \tau}}{T\Omega^2} \sum_{m=1}^{\Omega} \sum_{n=1}^{\Omega} e^{j2\pi \tilde{s}_n f_d \tau_0} (U_1(\alpha - \\ (\tilde{s}_m - \tilde{s}_n) f_d) + U_2(\alpha - (\tilde{s}_m - \tilde{s}_n) f_d)), & |\tau| \geq T, \end{cases} \tag{2.9}$$

$$\kappa = \{\frac{i}{T} | i, integer, M_r(\alpha,\tau) \neq 0\}, \tag{2.10}$$

[1]Here we consider only the signal component. The noise contribution needs to be added to the final result.

In these equations, μ equals -1 if $\tau < 0$, and 1 if $\tau \geq 0$, $\tilde{s}_m$ and $\tilde{s}_n$ are independent and identically distributed (i.i.d.) random variables, drawn from the alphabet $A_\Omega = \{\pm 1, \pm 3, ... \pm (\Omega - 1)\}$, $U_1(\alpha)$ and $U_2(\alpha)$ are the Fourier transforms of $u_T(t)u_T(t-\tau_0)$ and $u_T(t)u_T(t+\mu T-\tau_0)$, given respectively as

$$U_1(\alpha) = (T - |\tau_0|)sinc((T - |\tau_0|)\alpha)e^{-j\pi\alpha(T+\mu|\tau_0|)}, \tag{2.11}$$

$$U_2(\alpha) = |\tau_0|sinc(|\tau_0|\alpha)e^{-j\pi\alpha(T+\mu(|\tau_0|-T))}. \tag{2.12}$$

Proof of (2.8), (2.9), and (2.10)

By substituting (2.1) in (2.6), one can write the second-order time-varying moment of the received FSK signal as

$$m_{r_{FSK}}(t,\tau) = E\{a^2 e^{j2\pi\Delta f_c \tau} \sum_i \sum_k e^{j2\pi s_i f_d (t-iT)} e^{-j2\pi s_k f_d (t-kT-\tau)} \times u_T(t-iT)u_T(t-kT-\tau)\}. \tag{2.13}$$

The delay τ can be considered as $\tau = pT + \tau_0$, with $p = \lceil \tau/T \rceil$, if $\tau < 0$, and $p = \lfloor \tau/T \rfloor$, if $\tau \geq 0$. From (2.13), one can notice that the none-zero values of the product $u_T(t-iT)u_T(t-kT-\tau)$ can lead to non-zero $m_{r_{FSK}}(t,\tau)$. Furthermore, one can see that this product is non-zero in the following cases: $\tau_0 = 0$ (Figure 2.1) and $k = i - p$; $\tau_0 < 0$ (Figure 2.2) and either $k = i - p$ or $k = i - p + 1$; $\tau_0 > 0$ (Figure 2.3) and either $k = i - p$ or $k = i - p - 1$. By applying the above relationships between i and k to (2.13), one can further express the second-order moment of the received FSK signal as

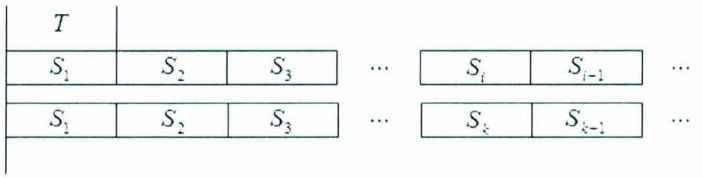

Figure 2.1: Relationship between the transmitted symbol and delayed symbol when $\tau = 0$.

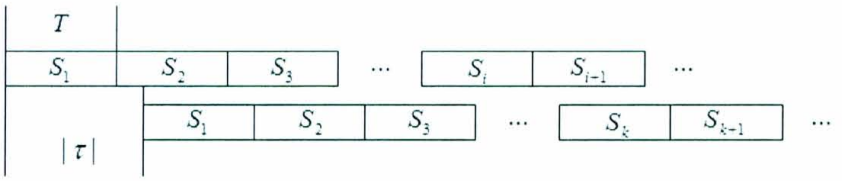

Figure 2.2: Relationship between the transmitted symbol and delayed symbol when $\tau < 0$.

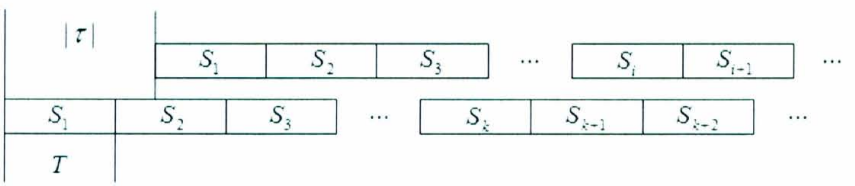

Figure 2.3: Relationship between the transmitted symbol and delayed symbol when $\tau > 0$.

$$m_{r_{FSK}}(t,\tau) = \begin{cases} a^2 e^{j2\pi\Delta f_c\tau} \sum_i E\{e^{j2\pi s_i f_d\tau_0} u_T(t-iT)u_T(t- \\ iT-\tau_0) + e^{j2\pi(s_i-s_{i-\mu})f_d(t-iT)} e^{j2\pi s_{i-\mu}f_d\tau_0} \\ \times u_T(t-iT)u_T(t-(i-\mu)T-\tau_0)\}, & |\tau| < T, \\ \\ a^2 e^{j2\pi\Delta f_c\tau} \sum_i E\{e^{j2\pi(s_i-s_{i-p})f_d(t-iT)} \\ \times e^{j2\pi s_{i-p}f_d\tau_0} u_T(t-iT)u_T(t-iT-\tau_0) \\ + e^{j2\pi(s_i-s_{i-p-\mu})f_d(t-iT)} e^{j2\pi s_{i-p-\mu}f_d\tau_0} \\ \times u_T(t-iT)u_T(t-(i-\mu)T-\tau_0)\}, & |\tau| \geq T, \end{cases} \tag{2.14}$$

where μ equals -1 if $\tau < 0$ and 1 if $\tau \geq 0$. By considering that the data symbols s_i, $s_{i-\mu}$, s_{i-p}, and $s_{i-p-\mu}$, are i.i.d. random variables with values drawn from $A_\Omega = \{\pm 1, \pm 3, ... \pm (\Omega - 1)\}$, the statistical average in (2.8) can be expressed, and after taking the Fourier transform of (2.8) and using (2.7), one can straightforwardly obtain (2.9) and (2.10). Note that $U_1(\alpha)$ and $U_2(\alpha)$ in (2.9) are the Fourier transforms of the products $u_T(t)u_T(t-\tau_0)$ and $u_T(t)u_T(t+\mu T-\tau_0)$, which appear in (2.8).

2.3 MSK signal model and its cyclostationarity

2.3.1 MSK signal model

The received MSK signal affected by block fading and additive Gaussian noise can be expressed as

$$r_{MSK}(t) = ae^{j\phi}e^{j2\pi\Delta f_c t}\sum_i e^{j2\pi s_i f_d(t-iT)}e^{j\frac{1}{2}\pi\sum_{n=-\infty}^{i-1}s_n}u_T(t-iT) + w(t), \tag{2.15}$$

s_i is the data symbol transmitted during the ith period, which takes values from the alphabet $A_{MSK} = \{-1, 1\}$ with equal probability, and $h = 2f_dT$ is the modulation index which equals $\frac{1}{2}$ for MSK signal.

2.3.2 First-order cyclostationarity of MSK signal

According to (2.2) and (2.15), the first-order moment of the received MSK signal is given by

$$m_{r_{MSK}}(t) = ae^{j\phi}e^{j2\pi\Delta f_c t}\sum_i E\{e^{j2\pi s_i f_d(t-iT)}\}\prod_{n=-\infty}^{i-1}E\{e^{j\frac{1}{2}\pi s_n}\}u_T(t-iT). \tag{2.16}$$

As $s_n \in A_{MSK} = \{-1, 1\}$, it is obvious that $E\{e^{j\frac{1}{2}\pi s_n}\} = 0$, which implies the nullity of $m_{r_{MSK}}(t)$. Thus, the MSK signal does not exhibit first-order cyclostationarity.

2.3.3 Second-order cyclostationarity of MSK signal

For the received MSK signal, the second-order time-varying moment, CM, and set of CFs are given in (2.17), (2.18), and (2.19), respectively. The proof is subsequently provided.

$$m_{r_{MSK}}(t,\tau) = \begin{cases} \frac{a^2 e^{j2\pi\Delta f_c \tau}}{4} \sum_i \sum_{m=1}^{2} \sum_{n=1}^{2} e^{j2\pi(\tilde{s}_m - \tilde{s}_n) f_d (t-iT)} e^{j\frac{1}{4}\pi(\tilde{s}_m - \tilde{s}_n)(1-\mu)} \\ \times e^{j2\pi \tilde{s}_n f_d \tau_0} e^{-j\frac{1}{2}\pi \tilde{s}_n} u_T(t - iT) u_T(t - iT - \tau_0), & T \le |\tau| < 2T, \\ \\ \frac{a^2 e^{j2\pi\Delta f_c \tau}}{4} \sum_i \sum_{m=1}^{2} \sum_{n=1}^{2} e^{j2\pi \tilde{s}_m f_d \tau_0} u_T(t - iT) u_T(t - iT - \tau_0) \\ + e^{j2\pi(\tilde{s}_m - \tilde{s}_n) f_d (t-iT)} e^{j\frac{1}{4}\pi(\tilde{s}_m - \tilde{s}_n)(1-\mu)} e^{j2\pi \tilde{s}_n f_d \tau_0} \\ \times u_T(t - iT) u_T(t - (i-\mu)T - \tau_0), & 0 \le |\tau| < T, \\ \\ 0, & otherwise, \end{cases} \tag{2.17}$$

$$M_{r_{MSK}}(\alpha,\tau) = \begin{cases} \frac{a^2 e^{j2\pi\Delta f_c \tau}}{4T} \sum_{m=1}^{2}\sum_{n=1}^{2} e^{j\frac{1}{4}\pi(\tilde{s}_m-\tilde{s}_n)(1-\mu)} e^{j2\pi\tilde{s}_n f_d \tau_0} e^{-j\frac{1}{2}\pi\tilde{s}_n} \\ \times U_1(\alpha-(\tilde{s}_m-\tilde{s}_n)f_d), & T \le |\tau| < 2T, \\ \frac{a^2 e^{j2\pi\Delta f_c \tau}}{4T} \sum_{m=1}^{2}\sum_{n=1}^{2} e^{j2\pi\tilde{s}_m f_d \tau_0} U_1(\alpha) + e^{j\frac{1}{4}\pi(\tilde{s}_m-\tilde{s}_n)(1-\mu)} \\ \times e^{j2\pi\tilde{s}_n f_d \tau_0} U_2(\alpha-(\tilde{s}_m-\tilde{s}_n)f_d), & 0 \le |\tau| < T, \\ 0, & otherwise, \end{cases} \tag{2.18}$$

$$\kappa = \{\frac{i}{T} | i, integer, M_{r_MSK}(\alpha,\tau) \neq 0\}, \tag{2.19}$$

Proof of (2.17), (2.18), and (2.19)

By substituting (2.15) in (2.6), one can write the second-order time-varying moment of the received MSK signal as

$$\begin{aligned} m_{r_{MSK}}(t,\tau) = E\{a^2 e^{j2\pi\Delta f_c \tau} \sum_i \sum_k e^{j2\pi s_i f_d (t-iT)} e^{j\frac{1}{2}\pi\sum_{n=-\infty}^{i-1} s_n} \\ \times e^{-j2\pi s_k f_d (t-kT-\tau)} e^{-j\frac{1}{2}\pi\sum_{q=-\infty}^{k-1} s_q} u_T(t-iT) u_T(t-kT-\tau)\}. \end{aligned} \tag{2.20}$$

As in (2.20), none-zero $m_{r_{MSK}}(t,\tau)$ is obtained when the product $u_T(t-iT)u_T(t-kT-\tau)$ is none-zero. This is similar to the proof for FSK signal second-order time-varying moment. Thus, we apply the same relation between i and k in Section (2.2.3): $\tau_0 = 0$, and $k = i-p$; $\tau_0 < 0$, and either $k = i-p$ or $k = i-p+1$; $\tau_0 > 0$, and either $k = i-p$ or $k = i-p-1$, and (2.20) can be further expressed as

$$
m_{r_{MSK}}(t,\tau) = \begin{cases}
a^2 e^{j2\pi\Delta f_c \tau} \sum_i E\{ e^{j2\pi(s_i - s_{i-p}) f_d (t-(i+1)T)} e^{j2\pi s_{i-p} f_d \tau_0} \\
\times e^{-j\frac{1}{2}\pi \sum_{n=i+1}^{i-p} s_n} u_T(t-iT) u_T(t-iT-\tau_0) \\
+ e^{j2\pi(s_i - s_{i-p+1}) f_d (t-(i+1)T)} e^{j2\pi s_{i-p+1} f_d \tau_0} e^{-j\frac{1}{2}\pi \sum_{n=i+1}^{i-p} s_n} \\
\times u_T(t-iT) u_T(t-(i+1)T-\tau_0)\}, & \tau < 0, \\
a^2 e^{j2\pi\Delta f_c \tau} \sum_i E\{ e^{j2\pi(s_i - s_{i-p}) f_d (t-iT)} e^{j2\pi s_{i-p} f_d \tau_0} \\
\times e^{j\frac{1}{2}\pi \sum_{n=i-p}^{i-1} s_n} u_T(t-iT) u_T(t-iT-\tau_0) \\
+ e^{j2\pi(s_i - s_{i-p-1}) f_d (t-iT)} e^{j2\pi s_{i-p-1} f_d \tau_0} e^{j\frac{1}{2}\pi \sum_{n=i-p}^{i-1} s_n} \\
\times u_T(t-iT) u_T(t-(i-1)T-\tau_0)\}, & \tau \geq 0.
\end{cases} \tag{2.21}
$$

By considering that data symbols s_i are i.i.d. random variables and $E\{e^{\pm j\frac{1}{2}\pi s_i}\} = 0$, the second-order moment of the received MSK signals can be further written as

$$
m_{r_{MSK}}(t,\tau) = \begin{cases}
a^2 e^{j2\pi\Delta f_c \tau} \sum_i E\{ e^{j2\pi(s_i - s_{i-\mu}) f_d (t-iT)} e^{j\frac{1}{4}\pi(s_i - s_{i-\mu})(1-\mu)} \\
\times e^{j2\pi s_{i-\mu} f_d \tau_0} e^{-j\frac{1}{2}\pi s_{i-\mu}} u_T(t-iT) u_T(t-iT-\tau_0)\}, & T \leq |\tau| < 2T, \\
a^2 e^{j2\pi\Delta f_c \tau} \sum_i E\{ e^{j2\pi s_i f_d \tau_0} u_T(t-iT) u_T(t-iT-\tau_0) \\
+ e^{j2\pi(s_i - s_{i-\mu}) f_d (t-iT)} e^{j\frac{1}{4}\pi(s_i - s_{i-\mu})(1-\mu)} e^{j2\pi s_{i-\mu} f_d \tau_0} \\
\times u_T(t-iT) u_T(t-(i-\mu)T-\tau_0)\}, & 0 \leq |\tau| < T, \\
0, & otherwise.
\end{cases} \tag{2.22}
$$

By considering that the data symbols s_i are i.i.d. random variables with values drawn from $A_{MSK} = \{-1, 1\}$, (2.17) can be easily obtained, and after taking the Fourier transform of (2.17) and using (2.7), one can straightforwardly reach (2.18) and (2.19).

2.4 Summary

In this chapter we present the mathematical models of the FSK and MSK signals. These are considered to be affected by block fading, additive Gaussian noise, and frequency offset. Furthermore, the analytical expressions for the first- and second-order cyclic moments and associated cycle frequencies of the FSK and MSK signals are obtained.

Chapter 3

Proposed algorithms

3.1 Introduction

The cyclostationary properties of signals have been explored for modulation classification and parameter estimation for more than two decades [16]- [17]. The advantage of cyclostationarity-based approaches is that they do not require preprocessing, such as timing and carrier recovery. In this chapter, we exploit the cyclic statistics of FSK and MSK signals to propose signal classification and parameter estimation algorithms. The proposed algorithms are able to classify received FSK and MSK signals affected by block fading and additive Gaussian noise, as well as to estimate the tone frequency spacing and symbol period of FSK signals.

3.2 First-order cyclostationarity based FSK signal classification and tone frequency estimation

The first-order CM magnitude of received FSK signals is shown in Figure. 3.1. As in the figure, peaks of $|m_r^K(\alpha')|$ are obtained at CFs, and insignificant magnitudes are

at frequencies other than the CFs. The number of first-order CFs is equal to two, four, and eight, for 2-FSK, 4-FSK, and 8-FSK signals, respectively. The proposed algorithm in this section relies on the number and position of the first-order CFs. The signal is applied to the algorithm input after being normalized to the root square of the received power. Accordingly, the normalization factor needs to be included in the previous expressions for the first-order CM. From (2.5), the following properties of the first-order CFs can be observed:

- (P1) The number of CFs equals the modulation order;
- (P2) The distance between adjacent CFs equals the tone frequency spacing;
- (P3) The distance between any two CFs is an integer multiple of the tone frequency spacing. We refer to this property as to the integer multiple relationship (IMR).

A flowchart of the proposed algorithm is depicted in Figure. 3.2; this consists of six steps, as follows:

Step 1: Selection of candidate frequencies. Since the CM magnitudes at CFs are significant, the frequencies for which the CM magnitude exceeds a cutoff value V_{co} [17] are selected as candidates. If the number of selected candidates, $N_{\mathscr{C}}$ is below 2 (i.e., the minimum FSK modulation order), an adaptive procedure for setting V_{co} based on the bisection method [33] is triggered. This procedure ends when a desired number of candidates is selected, which equals the maximum expected FSK modulation order, Ω_{max}.

Step 2: Local maximum refinement. We retain the adjacent candidates which are located at a distance greater than a minimum allowable distance $d_{\mathscr{C}}$. This is determined using the property (P2) provided above, and equals the ratio between the single-side signal bandwidth and Ω_{max}. For adjacent candidates placed at a distance below $d_{\mathscr{C}}$, the candidate with the higher CM magnitude is retained.

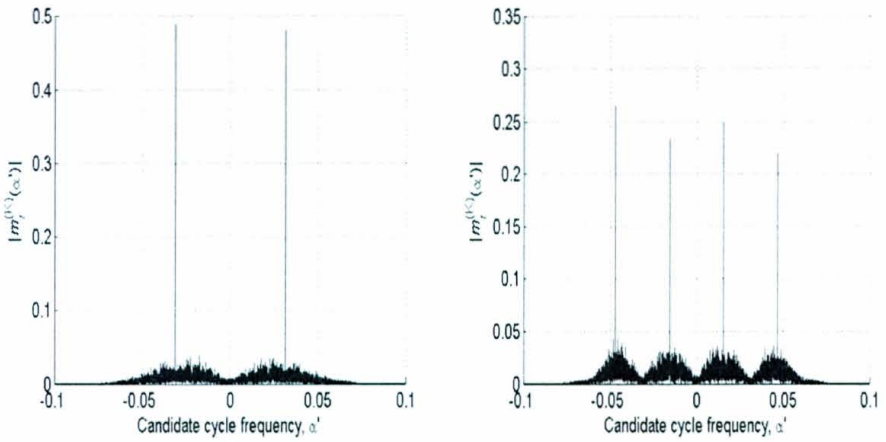

(a) 2-FSK

(b) 4-FSK

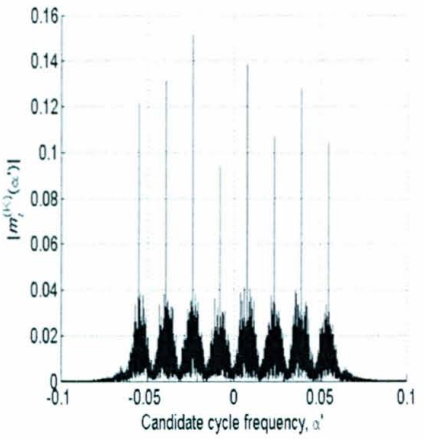

(c) 8-FSK

Figure 3.1: The magnitudes of the first-order estimated CM of the FSK signal, for (a) 2-FSK, (b) 4-FSK, and (c) 8-FSK.

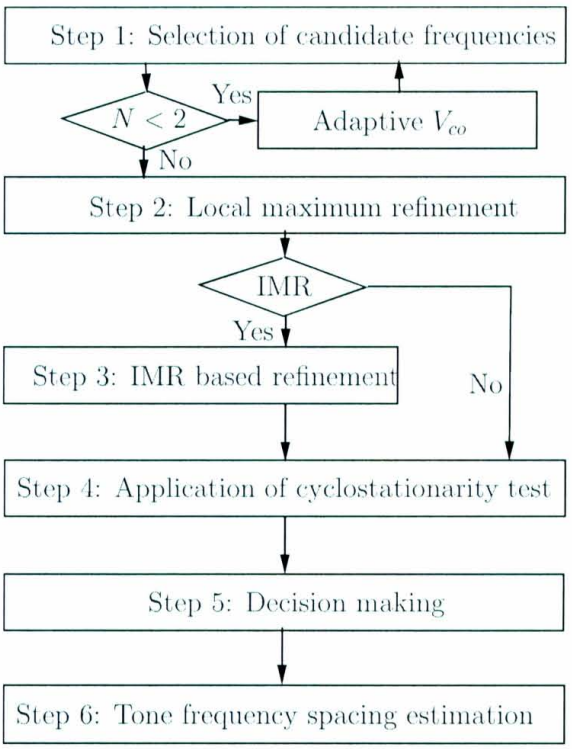

Figure 3.2: Flowchart of the proposed algorithm.

Step 3: IMR based refinement. The distances between pairs of candidate frequencies selected in Step 2 are calculated, and the IMR is verified (see property (P3) above). If the IMR is satisfied, the corresponding frequency candidates are retained. Furthermore, based on the fact that CFs are separated by equal distances, the position of missing frequencies can be inferred, and these are included as candidates. If the CF IMR property is not satisfied by any of the candidate frequencies, Step 3 is skipped.

Step 4: Application of a cyclostationarity test. The cyclostationarity test proposed in [17] is used to check if the previously selected candidate frequencies are CFs. A first-order CM based statistic value is estimated for each candidate CF and compared to a threshold, Γ which is determined from the probability of declaring that a candidate is a CF when it is not (P_{fa}). If the statistic value exceeds the threshold, the

corresponding candidate is declared a CF.

Step 5: Modulation order determination. The decision on the FSK modulation order is based on the number and position of the first-order CFs. The received signal is decided to be 2-FSK when two first-order CFs appearing on different sides of the central frequency are detected. Further, the received signal is considered to be Ω-FSK ($\Omega = 2^m, \Omega \geq 4$) if at least $2^{m-1}+1$ out of the Ω first-order CFs are detected and the distances satisfy the IMR condition. The output is either the modulation order or "Cannot decide." The latter decision is made if either the CF number or the CF position conditions are not satisfied.

Step 6: Tone frequency spacing estimation. The minimum distance between adjacent CFs is calculated. Note that for Ω-FSK ($\Omega = 2^m, \Omega \geq 4$) signals, although some CFs may be missed, since at least $2^{m-1}+1$ CFs are utilized, the minimum distance between adjacent CFs provides the tone frequency spacing.

3.3 Second-order cyclostationarity based FSK symbol period estimation algorithm

From (2.9) one can notice that the magnitude of $M_r(\alpha,\tau)$ depends on α, T, A_Ω, $U_1(.)$, and $U_2(.)$. For example, for $\alpha = 0$, $|M_r(0,\tau)|$ is

$$|M_r(0,\tau)| = \begin{cases} \frac{a^2}{T\Omega}\left|\sum_{n=1}^{\Omega} e^{j2\pi\tilde{s}_n f_d \tau_0}\left(U_1(0) + \frac{1}{\Omega}\sum_{m+1}^{\Omega} U_2((\tilde{s}_n - \tilde{s}_m)f_d)\right)\right|, \\ \qquad\qquad |\tau| < T, \\ \frac{a^2}{T\Omega^2}\left|\sum_{m=1}^{\Omega}\sum_{m=1}^{\Omega} e^{j2\pi\tilde{s}_n f_d \tau_0}\left(U_1((\tilde{s}_n - \tilde{s}_m)f_d)\right.\right. \\ \left.\left.+U_2((\tilde{s}_n - \tilde{s}_m)f_d)\right)\right| \qquad |\tau| \geq T. \end{cases} \tag{3.1}$$

It is noteworthy that $|M_r(0,\tau)_{2,1}|$ exhibits peaks if either $e^{j2\pi\tilde{s}_n f_d\tau_0} = 1$ or $e^{j2\pi\tilde{s}_n f_d\tau_0} = -1$ for $\tilde{s}_n$, n=1,2,..., Ω; this is obtained for $\tau_0 = v(2f_d)^{-1}$, v integer. We can further express (3.1) for different modulations. For example, one can easily show that for 2-FSK (3.1) becomes

$$|M_{2\text{-FSK}}(0,\tau)| = \begin{cases} \frac{a^2}{T}|U_1(0)cos(2\pi f_d\tau_0) + \frac{1}{2}U_2(0)cos(2\pi f_d\tau_0) \\ +\frac{1}{2}U_2(2f_d)e^{j2\pi f_d\tau}|, & |\tau| < T, \\ \\ \frac{a^2}{T}|\frac{1}{2}U_1(0)cos(2\pi f_d\tau_0) + \frac{1}{2}U_2(0)cos(2\pi f_d\tau_0) \\ +\frac{1}{2}U_1(2f_d)e^{j2\pi f_d\tau_0} + \frac{1}{2}U_2(2f_d)e^{j2\pi f_d\tau_0}|, & |\tau \geq T|. \end{cases} \tag{3.2}$$

Figure. 3.3 shows $|M_{2\text{-FSK}}(0,\tau)|/|M_{2\text{-FSK}}(0,0)|$ versus τ, with the signal parameters as provided in Chapter 4; this confirms the positions of the peaks. The proposed symbol period estimation algorithm relies on the existence of peaks in $|M_r(0,\tau)|$, at delays $\tau = v(2f_d)^{-1}$, v integer, i.e., $P_v = |M_r(0, v(2f_d)^{-1}_{2,1})|$. For such delays, by using (2.11) and (2.12), one can find that $U_1(0) = T - |\tau_0|$, $U_2(0) = |\tau_0|$, and $U_1((\tilde{s}_n - \tilde{s}_m)f_d) = U_1((\tilde{s}_n - \tilde{s}_m)f_d) = 0$ unless $\tilde{s}_n = \tilde{s}_m$, and

$$|M_r(0, v(2f_d)^{-1})| = \begin{cases} a^2(1 - \frac{\Omega-1}{T\Omega}|v(2f_d)^{-1}|), & |v(2f_d)^{-1}| < T, \\ \\ \frac{a^2}{\Omega}, & |v(2f_d)^{-1}| \geq T. \end{cases} \tag{3.3}$$

If $|v(2f_d)^{-1}| < T$, the peak value decreases with increasing $|v(2f_d)^{-1}|$, whereas if $|v(2f_d)^{-1} \geq T|$, the peak values is a constant equal to a^2/Ω. It is noteworthy that the first constant value of the peaks is attained at delay T. Thus, by distinguishing the pattern of peak values, we can find the position of the first constant peak value, and consequently obtain the symbol period estimate.

The leader-follower clustering approach [25] is employed to distinguish different pat-

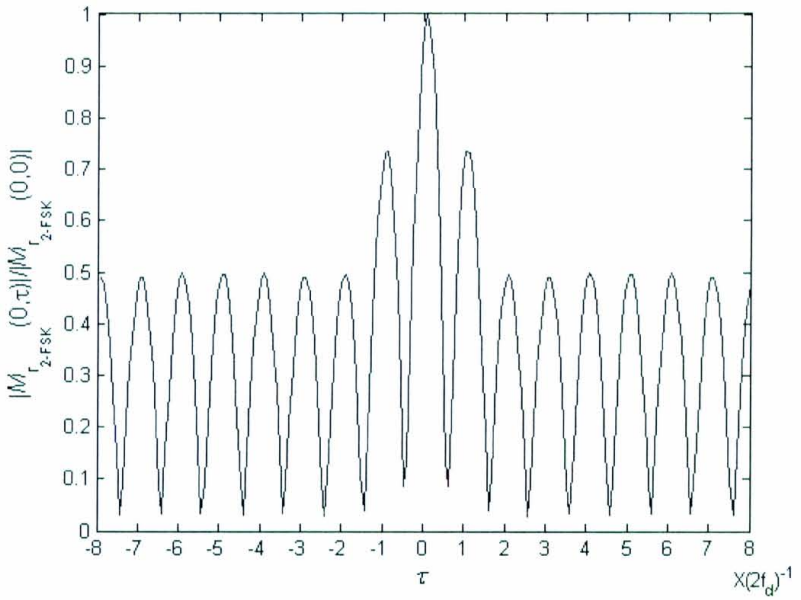

Figure 3.3: Normalized magnitude of the 2-FSK signal second-order CM at zero CF, with no noise and fading effect.

terns of the peak values. First, the last obtained peak value is selected as a cluster center. If the difference between a peak value and the cluster center is less than a preset threshold ε, this value is categorized to belonging to the constant peak value pattern, and the cluster center is updated by the mean value of the existing members of this pattern. This procedure continues until no peak values can be categorized to the cluster center. According to (3.3), the constant peak value pattern starts at $|\tau| = T$. Thus, we estimate the symbol period by calculating the minimum $|\tau|$ of the peak values belonging to this pattern. The proposed algorithm is formally stated below.

Step 1: The received signal is down-converted, band-limited through filtering, over-

sampled, and normalized by the square root of the received signal power [1].

Step 2: Estimate the absolute value of the second-order CM of the received signal at zero CF over a large enough delay range, and the peak values are retained, $P_v = |\hat{M}_r(0, v(2f_d)^{-1})|$, where v=0, 1, 2,..., $N-1$, with N as the number of obtained peaks.

Step 3: Initialize the cluster center to the last obtained peak value, $P_{\mathscr{C}} = P_{N-1}$, and add P_{N-1} into the set of constant peak value pattern, $\mathscr{C}$, which is initialized as $\mathscr{C} = \phi$

Step 4: Calculate the minimum difference between the cluster center and all the peak values, except for the members in $\mathscr{C}$,

$$d_i = argmin_{P_i \notin \mathscr{C}} |P_{\mathscr{C}} - P_i|. \tag{3.4}$$

Step 5: If $d_i \leq \varepsilon$, add P_i into the set $\mathscr{C}$, update the cluster center by the mean value of the members in $\mathscr{C}$, then go back to step 4. If $d_i > \varepsilon$, go to step 6.

Step 6: The symbol period of the received FSK signal is estimated as

$$\hat{T} = argmin_{P_v \notin \mathscr{C}} \{|v(2f_d)^{-1}|\}. \tag{3.5}$$

3.4 Joint classification of MSK and FSK signals

From (2.5) and (2.16), one can notice that the number of first-order CFs for the FSK signal equals the modulation order, whereas the MSK signal does not have first-order CFs. Thus, it is straightforward to distinguish MSK and FSK signals according to

[1] Note this is equivalent to normalizing the second-order CM of the received signal to the received signal power, $|M_r(0.0)|$

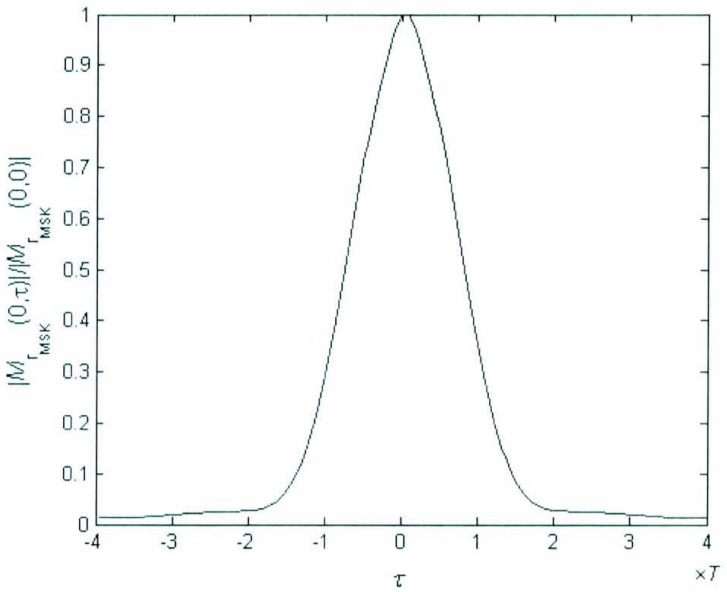

Figure 3.4: Normalized magnitude of the MSK signal second-order CM at zero CF.

the number of first-order CFs. However, the nullity of first-order cyclostationarity for MSK signal is obtained when considering an infinite number of symbols. If the observation period is short, the received MSK signal may also exhibit significant values in the first-order CM magnitude, and therefore leads to a misclassification. Thus, we additionally apply the second-order cyclostationary properties of the received MSK

and FSK signals to improve the classification accuracy. According to (2.18), we have

$$|M_{r_{MSK}}(0,\tau)| = \begin{cases} \frac{a^2}{4T}\Big|\sum_{m=1}^{2}\sum_{n=1}^{2} e^{j\frac{1}{4}\pi(\tilde{s}_m-\tilde{s}_n)(1-\mu)} e^{j2\pi\tilde{s}_n f_d\tau_0} e^{-j\frac{1}{2}\pi\tilde{s}_n} \\ \times U_1((\tilde{s}_n-\tilde{s}_m)f_d)\Big|, & T \le |\tau| < 2T, \\ \frac{a^2}{4T}\sum_{m=1}^{2}\Big|\sum_{n=1}^{2} e^{j2\pi\tilde{s}_m f_d\tau_0} U_1(0) + e^{j\frac{1}{4}\pi(\tilde{s}_m-\tilde{s}_n)(1-\mu)} \\ \times e^{j2\pi\tilde{s}_n f_d\tau_0} U_2((\tilde{s}_n-\tilde{s}_m)f_d)\Big|, & 0 \le |\tau| < T, \\ 0, & otherwise, \end{cases} \tag{3.6}$$

When compared with $|M_{r_{\mathrm{FSK}}}(0,\tau)|$, which is introduced in the previous section, $|M_{r_{\mathrm{MSK}}}(0,\tau)|$ does not exhibit a series of constant peak values when $\tau \ge T$ (see Figure 3.4). Such a difference is used to further distinguish MSK and FSK signals. The flowchart of the proposed joint classification algorithm is shown in Figure 3.5; this consists of two stages.

In the first stage, the first-order cyclostationarity of the received signal, which is normalized to the root square of the received power, is investigated. As in Figure 3.5 (b), we first select candidate frequencies based on a preset cutoff value. The following steps, such as the Local maximum refinement, IMR based refinement, and Cyclostationarity test, further examine if the selected candidates are real first-order CFs. The received signal is considered to be Ω-FSK ($\Omega = 2^m, \Omega \ge 4$) if at least $2^{m-1}+1$ out of the Ω first-order CFs are detected and the distances satisfy the IMR condition. Otherwise, the proposed algorithm goes to the second stage.

In the second stage, we estimate the absolute value of the second-order CM of the received signal at zero CF over a large enough delay range, $|M_{r_{\mathrm{FSK}}}(0,\tau)|$, and the local maximum values of $|M_{r_{\mathrm{FSK}}}(0,\tau)|$ are selected. We take the last obtained local

maximum value as an initial cluster center, and use the Leader-follower clustering method; which is introduced in Section 3.2 [25], to group the local maximum values which are close to the cluster center. Then, we check if the neighbor distances between grouped local maximum values have IMR.

The received signal is considered to be Ω-FSK ($\Omega = 2^m, \Omega \geq 4$) if at least $2^{m-1} + 1$ out of the Ω first-order CFs are detected in the first stage and their distances satisfy the IMR condition (see Section 3.3). A received signal is considered to be 2-FSK if two first-order CFs appearing on different sides of the central frequency are detected in the first stage and the neighbor distances between grouped local maximum values in the second stage have the IMR property. A received signal is considered to be MSK signal if the IMR property is not satisfied in the second stage. The case "Otherwise" in the first stage occurs under the following conditions: less than two first-order CFs are detected, two first-order CFs appearing on the same side of the central frequency are detected, and more than two first-order CFs without IMR property are detected. For such case, if the neighbor distances between grouped local maximum values have IMR in the second stage, the output of the algorithm is "Cannot decide".

3.5 Summary

In this chapter, we exploit the cyclostationary properties of the FSK and MSK signals to propose three algorithms for signal classification and parameter estimation. Based on first-order cyclostationarity, we determine the modulation order and the tone frequency spacing of FSK signals. Based on the second-order cyclostationarity, we can further estimate the symbol period of FSK signals. Moreover, by combining the first- and second-order cyclostationarity, we distinguish FSK and MSK signals.

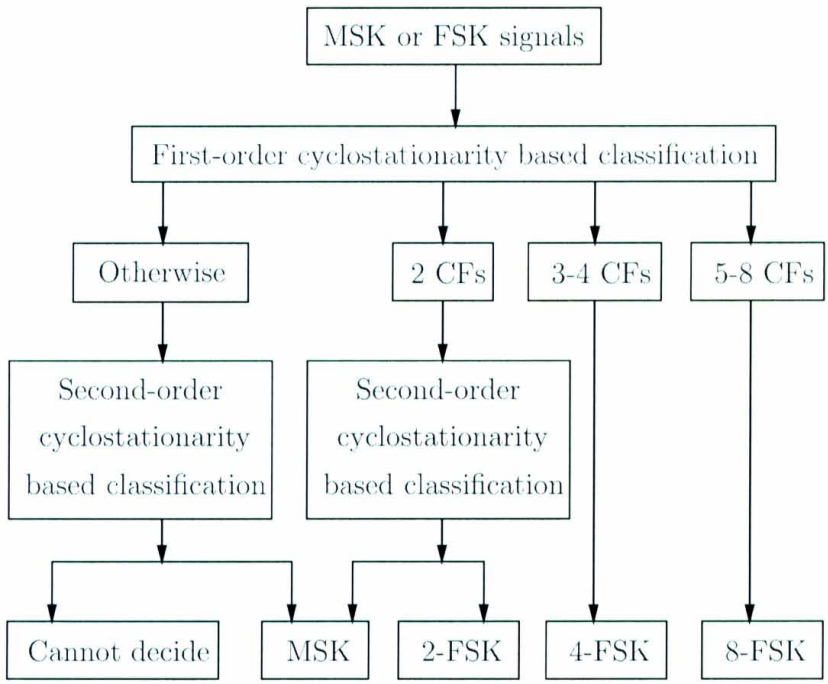

(a) Flowchart of the proposed classification algorithm

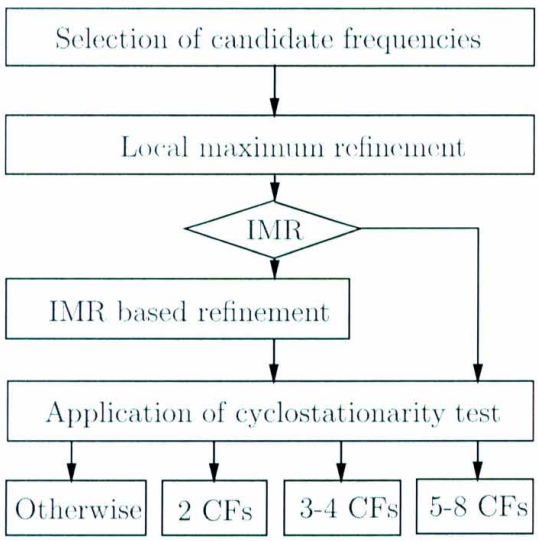

(b) First-order cyclostationarity based classification

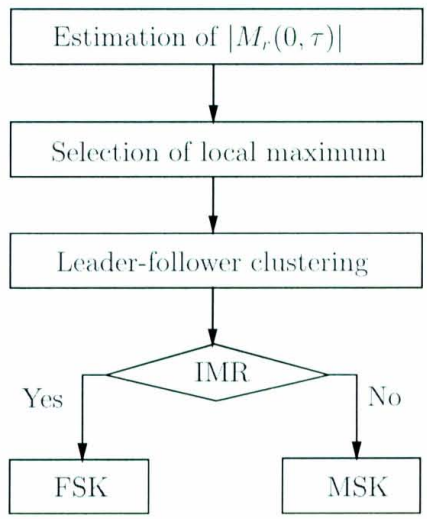

(c) Second-order cyclostationarity based classification

Figure 3.5: Joint MSK and FSK classification algorithm.

Chapter 4

Performance of proposed algorithms

4.1 Simulation setup

We consider MSK and FSK signals, Ω=2, 4, 8, $f_d = 1/T$, with the single-sided bandwidth equal 4 kHz (=Ω/T). The sampling rate f_s is 50 kHz, and the frequency offset Δf_c equals 250 Hz. A Butterworth low-pass filter of order 9 is used to remove out-of-band noise at the receiver. The -3dB bandwidth of this filter is set to 4 kHz, and the in-band SNR is considered. Unless otherwise mentioned, the observation period is 1 sec, which corresponds to 2000 MSK symbols, 2000 2-FSK symbols, 1000 4-FSK symbols, and 500 8-FSK symbols. The channel is Rayleigh fading with an average power of 1. For the classification and estimation algorithms, the performance is in terms of probability of correct classification, $P_c(\Omega\text{-FSK}|\Omega\text{-FSK})$ or $P_c(\text{MSK}|\text{MSK})$, and probability of correct estimation, P_{ce}; these are calculated based on 1,000 Monte Carlo trials.

4.2 Performance of the first-order cyclostationarity based FSK signal classification and tone frequency spacing estimation algorithm

4.2.1 The magnitude of the first-order CM estimate

The magnitude of the first-order CM estimate of 8-FSK signals is plotted in Figure. 4.1 to show the candidate frequencies for diverse SNRs. It is observed that the relevant peaks, which correspond to the CFs, are more predominant when compared with the noisy floor as the SNR increases. In addition, one can notice that for a very low SNR (e.g., -10 dB), the initial preset cutoff value does not allow the selection of enough candidates (see Figure. 4.1 (a)). In such a case, the mechanism to adaptively change the cutoff value is triggered, as described in the selection of candidate frequencies step, in Section 3.2. At higher SNRs (e.g., -5 dB) not all first-order CFs are selected (see Figure. 4.1 (b)); however, missing CFs can be recovered based on the CF properties mentioned in P2 and P3 (see Section 3.2). As the SNR increases further, (e.g., 0 dB) eight CFs can be exactly selected (see Figure. 4.1 (c)), and a further increase in the SNR can result in more than eight candidates (see Figure. 4.1 (d)). In the latter case, false candidates are rejected in the local maximum refinement step (see Section 3.2).

4.2.2 Initial cutoff value setup

Figure. 4.2 shows the probability of correct classification as a function of the initial cut-off value, V_{co}. Note that when V_{co} is low, the probability of correctly classifying 2-FSK and 4-FSK signals increases with increasing V_{co} (see Figure. 4.2 (a) and (b)), while the probability of classifying 8-FSK signals does not (see Figure. 4.2 (c)). This can be explained as follows. For a reduced V_{co}, more CF candidates are selected in

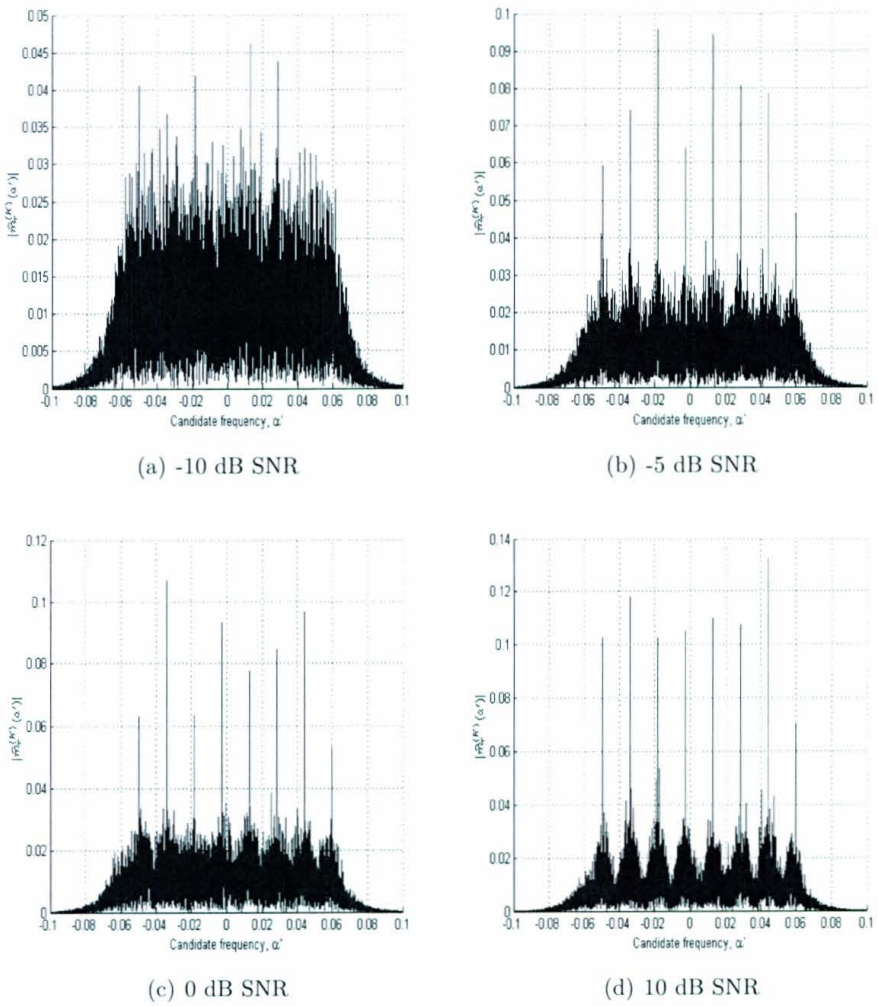

(a) -10 dB SNR

(b) -5 dB SNR

(c) 0 dB SNR

(d) 10 dB SNR

Figure 4.1: The magnitude of the first-order CM estimate of 8-FSK signals at (a) -10 dB SNR, (b) -5 dB SNR, (c) 0 dB SNR, and (d) 10 dB SNR.

the selection of candidate frequencies step (see Section 3.2). Those candidates which are very close to the CFs are rejected in local maximum refinement step; however, for signals with lower modulation orders there are still false CF candidates which pass local maximum refinement, which in turn lead to performance degradation. As V_{co} further increases, performance degradation occurs. This is because, at high V_{co} some of the CFs are missed even when an adaptive V_{co} search process is used if the minimum number of candidates is below the minimum modulation order (Ω = 2). We consider an initial cutoff value of 0.05, which provides a reasonably good probability of correct classification for different modulation types and at diverse SNRs.

4.2.3 Cyclostationarity test threshold setup

Table 4.1 and 4.2 provide the SNR required to achieve $P_c(\Omega - \text{FSK}|\Omega - \text{FSK})$=0.8 and $P_c(\Omega - \text{FSK}|\Omega - \text{FSK})$=0.9, Ω=2,4,8, with various values of the threshold, Γ, used in the cyclostationarity test of the proposed algorithm (see Section 3.2). As in the tables, for increased Γ, the required SNR tends to decrease for 2-FSK signals and increase for 8-FSK signals. For 4-FSK signals the required SNR exhibits a relative local optimum. This can be explained as follows. For 2-FSK signals, an incorrect decision is expected when the number of candidates passing the cyclostationarity test of the algorithm exceeds two, and, thus, a higher threshold is beneficial. On the other hand, an incorrect decision for the 8-FSK signals is obtained when an excessively high threshold results in the rejection of valid candidates when the cyclostationarity test is applied. Finally, both scenarios apply for 4-FSK signals. We select Γ = 5.9914 as providing a relatively good performance, $P_c(\Omega - \text{FSK}|\Omega - \text{FSK})$, Ω=2, 4, 8.

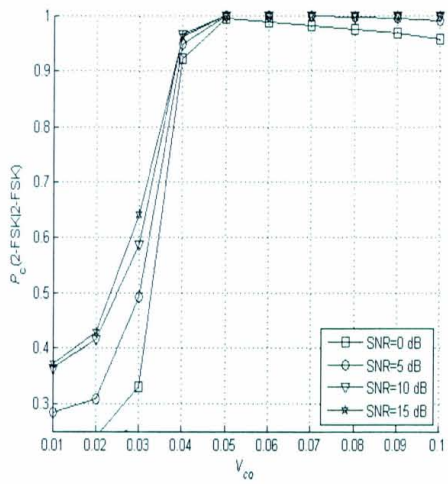

(a) 2-FSK

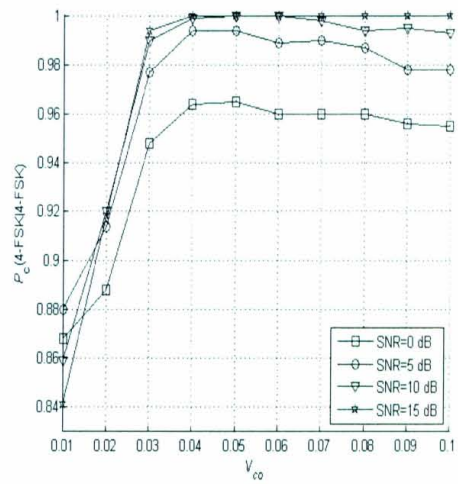

(b) 4-FSK

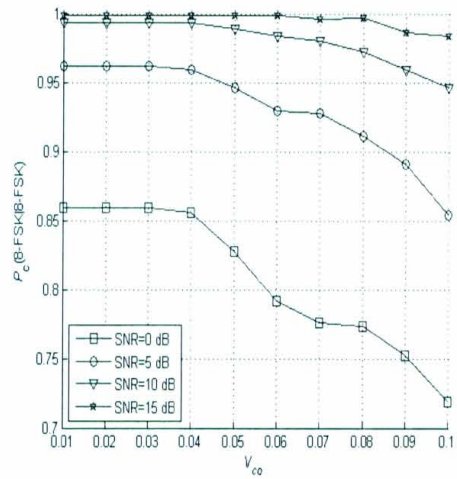

(c) 8-FSK

Figure 4.2: Probability of correct classification versus the cutoff value for (a) 2-FSK, (b) 4-FSK, and (c) 8-FSK signals at various SNRs.

Table 4.1: SNR (dB) required to achieve a $P_c(\Omega - \text{FSK}|\Omega - \text{FSK})$=0.8.

Ω \ Γ	4.60517	5.99147	7.37776	10.5966	13.816
2-FSK	-11.8	-11.8	-11.8	-12	-12.7
4-FSK	-7.1	-7.2	-7.2	-7.1	-6.3
8-FSK	-1.9	-1.9	-1.7	-1.1	0.2

Table 4.2: SNR (dB) required to achieve a $P_c(\Omega - \text{FSK}|\Omega - \text{FSK})$=0.9.

Ω \ Γ	4.60517	5.99147	7.37776	10.5966	13.816
2-FSK	-8.5	-8.5	-8.5	-8.6	-9.3
4-FSK	-3.6	-3.6	-3.6	-3.5	-2.9
8-FSK	1.6	1.6	1.7	2.1	3.2

4.2.4 FSK signal classification performance

Figure. 4.3 plots the probability of correct classification, $P_c(\Omega - \text{FSK}|\Omega - \text{FSK})$, Ω, 2, 4, 8, versus the SNR. The classification performance improves with increasing SNR; a probability of correct classification approaches 1 at 2, 9, and 13 dB SNR for Ω = 2, 4, and 8, respectively. Confusion matrices are provided in Table 4.3 (SNR = 0 dB) and Table 4.4 (SNR = 10 dB). Clearly, there are cases for which the algorithm cannot make a decision, especially under low SNR conditions. Also, miss-classification can occur, particularly for higher-order modulations. This is due to the miss-detection of CFs; and higher-order modulations are miss-classified as lower-order modulations. Moreover, Figure. 4.4 plots the 8-FSK signal classification performance of the proposed algorithm and that in [17]. Clearly, the proposed algorithm benefits significantly from the exploitation of the CF properties in the local maximum and IMR refinement steps.

Table 4.3: Confusion matrix for SNR=0 dB.

Output \ Input	2-FSK	4-FSK	8-FSK
2-FSK	993	14	18
4-FSK	0	957	12
8-FSK	0	0	869
Cannot decide	7	29	101

Table 4.4: Confusion matrix for SNR=10 dB.

Output \ Input	2-FSK	4-FSK	8-FSK
2-FSK	1000	0	2
4-FSK	0	999	1
8-FSK	0	0	993
Cannot decide	0	1	4

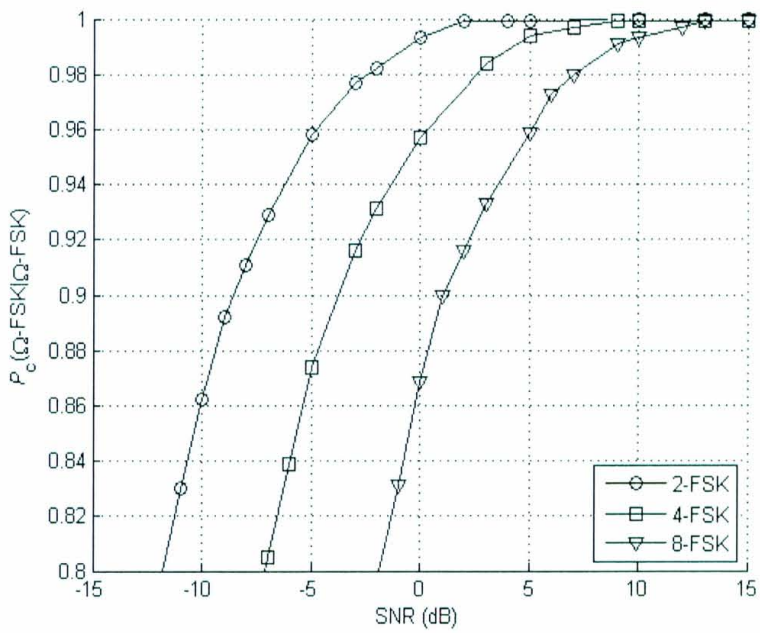

Figure 4.3: Classification performance versus SNR for Ω-FSK signals, $\Omega = 2, 4, 8$.

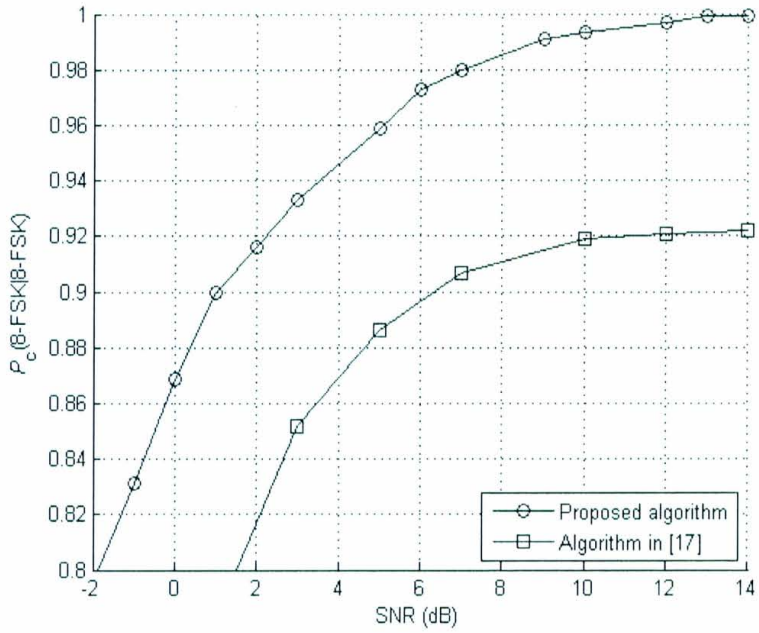

Figure 4.4: Classification performance comparison between the proposed algorithm and that in [17].

In Figure. 4.5, P_c(8-FSK|8-FSK) is shown versus SNR for different observation periods. As expected, a longer observation period leads to a better performance, as more accurate CM estimates are obtained. It is noteworthy that a good performance is achieved with relatively short observation periods.

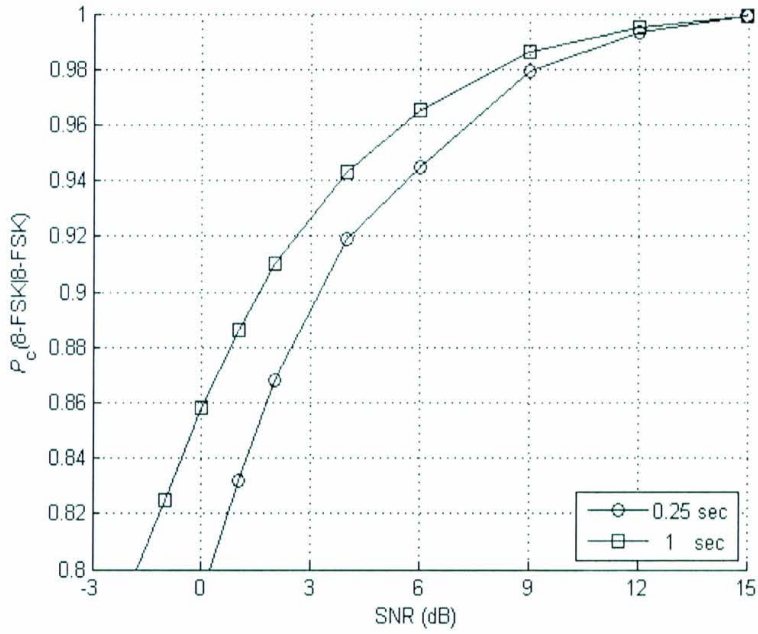

Figure 4.5: Classification performance versus SNR for 8-FSK with different observation periods.

In Figure. 4.6, the impact of the Ricean K factor on the performance of the proposed algorithm is studied. As expected, the performance improves as K increases; for $K \to \infty$, the performance approaches that in the AWGN channel.

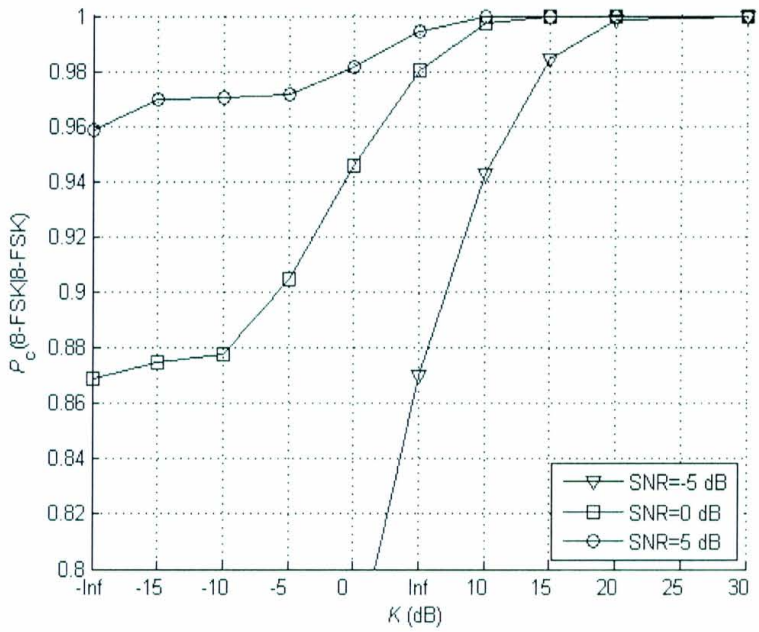

Figure 4.6: Classification performance versus Ricean K factor for 8-FSK, at -5 dB, 0 dB, and 5 dB SNR, respectively

4.2.5 Tone frequency spacing estimation performance

Estimation of the tone frequency spacing is carried out in the last step of the algorithm, after a decision on the modulation order is made (see Figure. 3.2). Hence, the decision on the modulation order affects the performance of the tone frequency spacing estimate. If the decision for the modulation order is "Cannot decide," then the algorithm cannot output an estimate for the tone frequency spacing. For 4-FSK and 8-FSK signals, a large error in the estimation of the tone frequency spacing comes from the wrong decision for the modulation order, e.g., if the decision is $\Omega = 2$ instead of $\Omega = 4$ or 8. On the other hand, for 2-FSK, errors in the tone frequency spacing estimation can also occur when the decision for the modulation order is correct; this

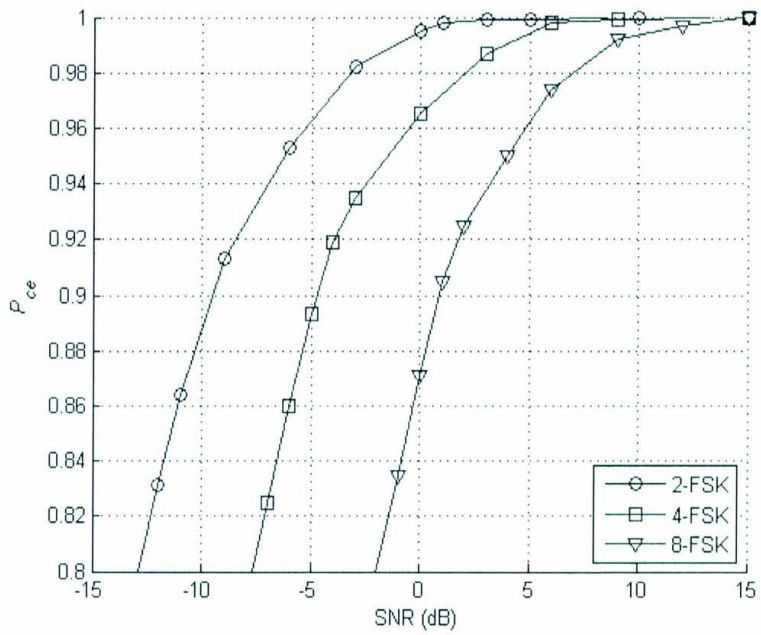

Figure 4.7: Probability of correct tone frequency spacing estimation versus SNR for Ω-FSK signals, $\Omega = 2, 4, 8$.

is due to the fact that IMR property, (P3), mentioned in Section 3.2 does not provide a strict constraint, unlike in 4-FSK and 8-FSK signals.

The probability of the tone frequency spacing estimate is plotted in Figure. 4.7 versus SNR, for 2-FSK, 4-FSK, and 8-FSK signals. As expected, a better estimation performance is achieved for lower orders, as a better classification performance is also achieved in such a case. Furthermore, results in Figure. 4.3 and 4.7 are close; this is expected, as correct estimation is obtained when classification makes right decision. For higher modulation order signals, the $P_{ce}(\Omega - \text{FSK})$ is slightly greater than $P_c(\Omega - \text{FSK}|\Omega - \text{FSK})$. This is attributed to the cases that miss-detection of CFs results in wrong classification decision whereas the distance between detected CFs still provides correct tone frequency spacing estimate.

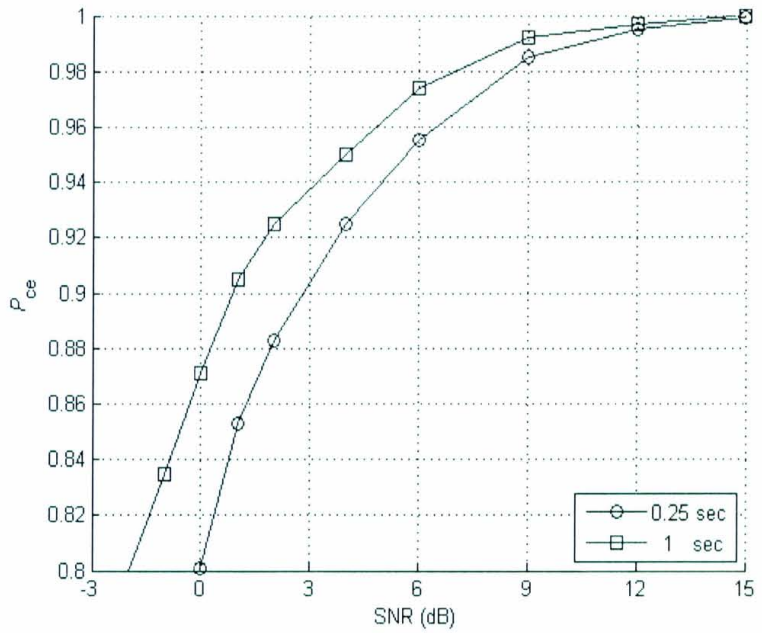

Figure 4.8: Probability of correct tone frequency spacing estimation versus SNR for 8-FSK signals with different observation periods.

Figure. 4.8 depicts the P_{ce} of the tone frequency spacing for 8-FSK signals with different observation periods. The proposed estimator performs well with a relatively short observation period, and the estimation accuracy improves as the observation period increases.

4.2.6 Receiver spatial diversity for FSK signal classification and tone frequency spacing estimation

Spatial diversity can be applied at the receive-side by utilizing the selection combining (SC) scheme to further improve the performance. The signal at the output of the

combiner is given by

$$r_{SC}(t) = r_l(t),\ l = \text{argmax}_{l=1,2,...,L} E\{|r_l(t)^2|\}, \tag{4.1}$$

where L represents the number of receive antennas, and $r_l(t)$ is the signal for the l-th antenna, $l = 1, 2, ..., L$.

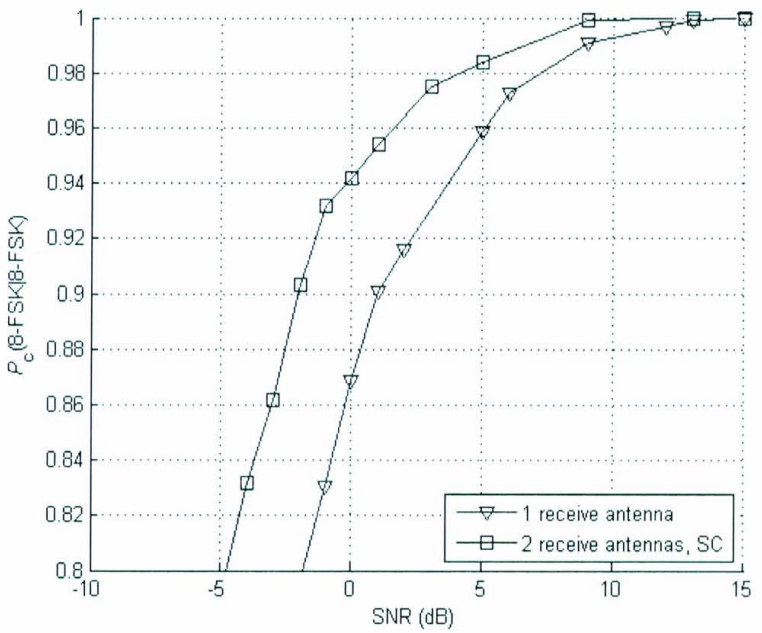

Figure 4.9: Classification performance versus SNR for 8-FSK with one and two receive antennas.

Figure. 4.9 shows the probability of correctly classifying 8-FSK signals when employing a single receive antenna and two receive antennas with selection combining, respectively. As expected, improved classification performance is achieved when exploiting spatial diversity. For example, a 3 dB SNR gain is achieved with two receive antennas when reaching a probability of correct classification of 0.9. Moreover, Fig-

ure. 4.10 compares the probability of correct tone frequency spacing estimation for 8-FSK signals when using a single antenna and two receive antennas with selection combining, respectively. As expected, the performance is improves. Since the combiner select the antenna with highes received signals power, channel estimation is not required when using SC.

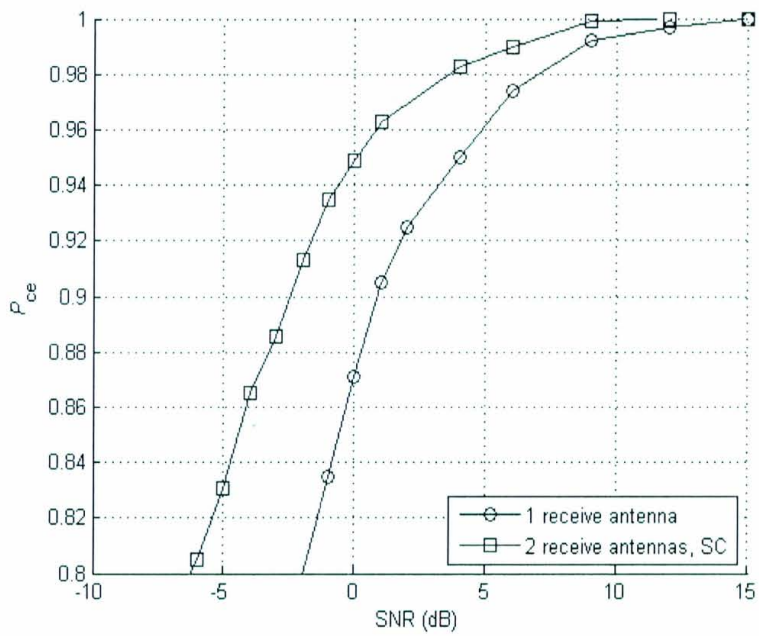

Figure 4.10: Probability of correct tone frequency spacing estimation versus SNR for 8-FSK signals with one and two receive antennas.

4.3 Performance of second-order cyclostationarity based FSK symbol period estimation algorithm

4.3.1 Setting the threshold value ε

Figure. 4.11 shows the probability of correct estimation, P_{ce}, as a function of the threshold value ε. Note that when ε is low, P_{ce} increases with increasing ε. This is because the peak value at delay $v(2f_d)^{-1} = T$ is less likely to be missed when using a greater threshold ε. However, as ε further increases, performance degradation occurs, since the peak values at delays $v(2f_d)^{-1} < T$ are wrongly included in the set of constant value pattern (see Section 3.3 for the algorithm description). We select a threshold value of 0.05, which provides a reasonable good P_{ce} for different modulation orders.

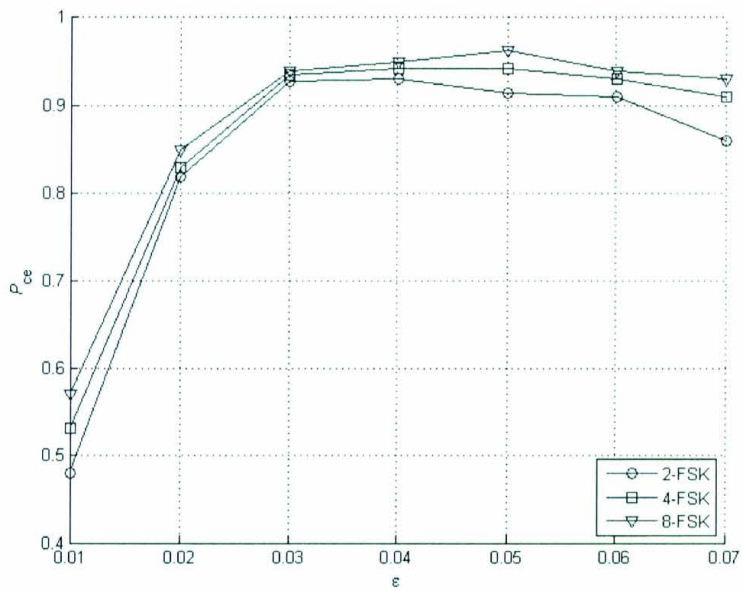

Figure 4.11: Probability of correct symbol period estimation versus the threshold value, ε, for 2-FSK, 4-FSK, and 8-FSK signals, at 5 dB SNR.

4.3.2 Symbol period estimation performance

The performance of correct symbol period estimation for different FSK signals versus SNR is shown in Figure. 4.12. The estimation performance improves as the modulation order increases. This is because for higher-order modulations, the difference between peak values at $|v(2f_d)^{-1}| \geq T$ and those at $|v(2f_d)^{-1}| < T$ is greater than for lower-order modulations, according to (3.3). Thus, the peaks patterns can be distinguished more easily, and the pattern clustering is more accurate.

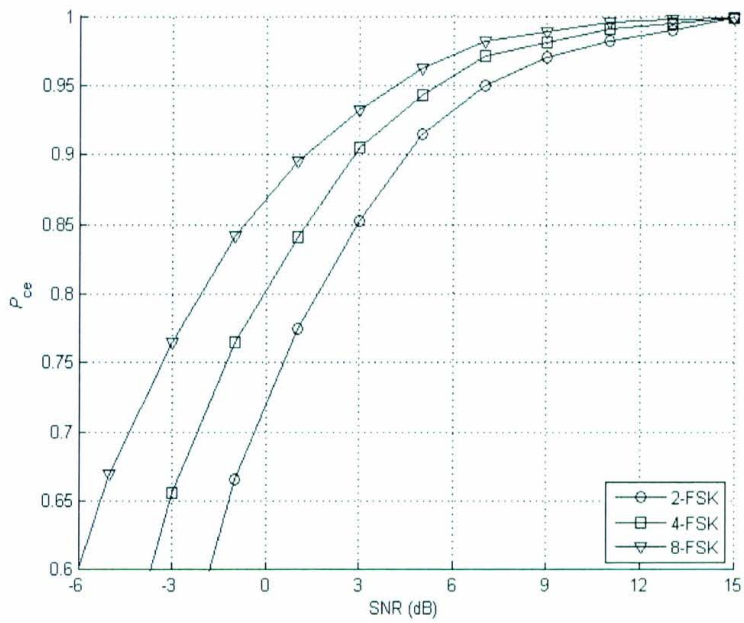

Figure 4.12: Probability of correct symbol period estimation versus SNR for Ω-FSK signals, $\Omega = 2, 4, 8$.

Figure. 4.13. shows the estimation performance for 2-FSK using different observation periods. As expected, a better performance is obtained with a longer observation period. Note that a reasonably good performance is obtained with relatively short

observation periods.

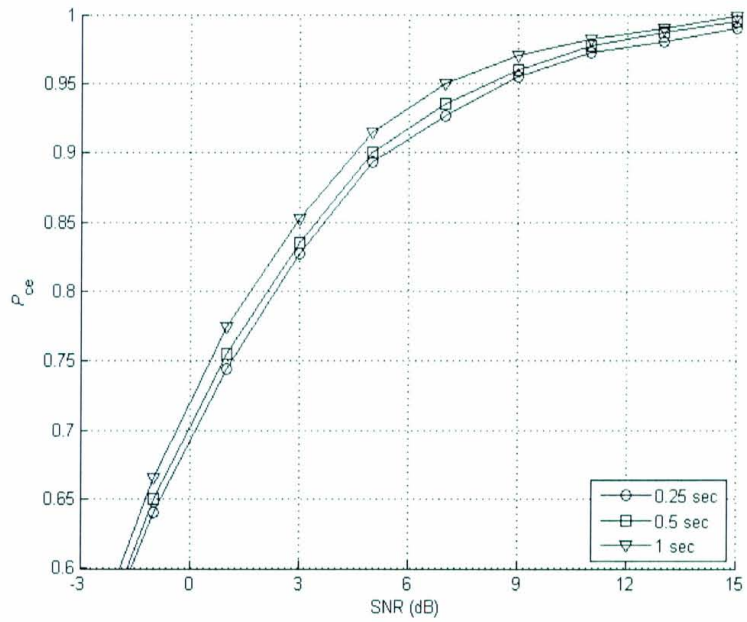

Figure 4.13: Probability of correct symbol period estimation for 2-FSK signals versus SNR with different observation periods.

Figure. 4.14 shows the probability of correctly estimating the symbol period for 2-FSK signals when employing different numbers of receive antennas with selection combining. As expected, an improved estimation performance is achieved when employing multiple antennas.

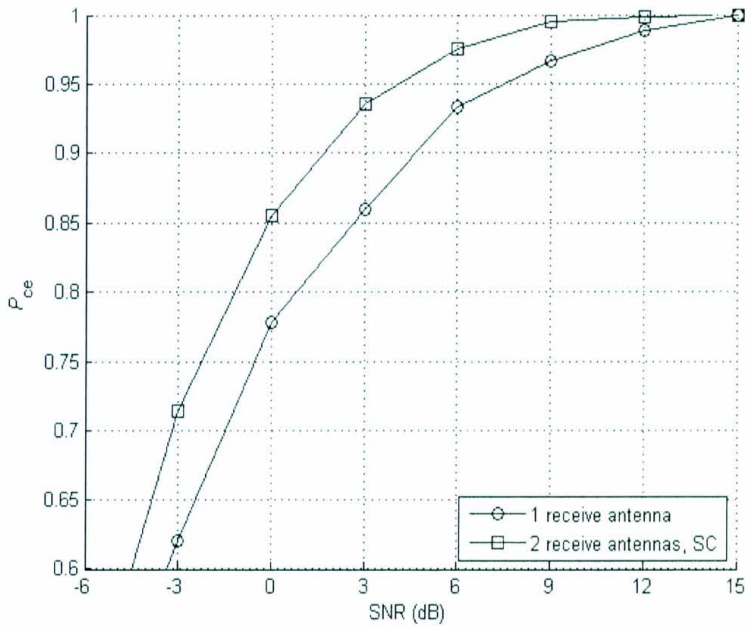

Figure 4.14: Probability of correct symbol period estimation for 2-FSK signals versus SNR with one and two antennas.

4.4 Performance of joint classification algorithm of MSK and FSK signals

The probability of correct classification, $P_c(i|i)$ i=2-FSK, 4-FSK, 8-FSK, and MSK, is shown in Figure 4.15. As shown in the figure, a P_c=0.8 for MSK signals is obtained at 2 dB SNR, and P_c approaches 1 at 18 dB SNR. Although the probability of correctly classifiying MSK signals is lower than that for FSK signals, a reasonable good performance is obtained.

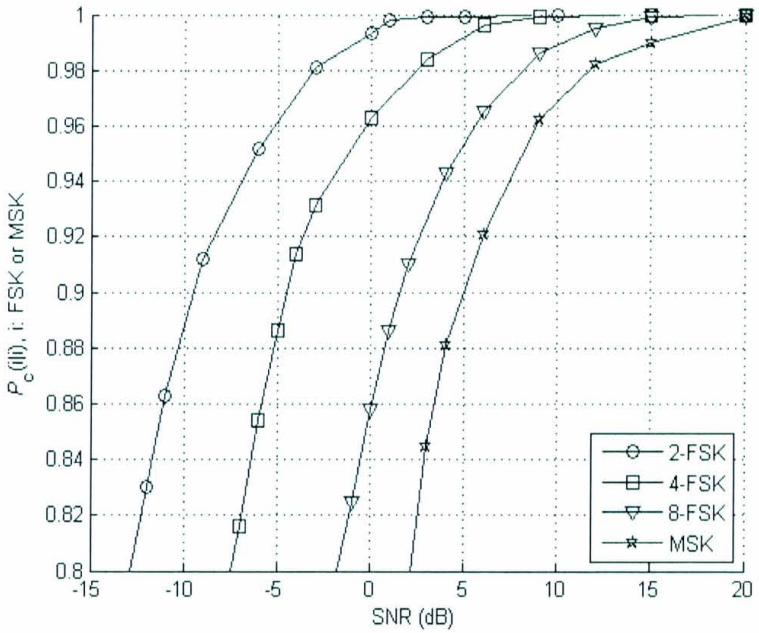

Figure 4.15: Classification performance versus SNR for FSK and MSK signals with 1 sec observation period.

Moreover, Figure 4.16 shows the performance of MSK signal classification using different observation periods. As expected, a longer observation period leads to a better performance, as more accurate CM estimates are obtained. Note that the effect of the observation period is more significant for MSK signal classification than for FSK signals. A longer observation period is required for MSK signal classification to obtain a performance similar to for FSK signals.

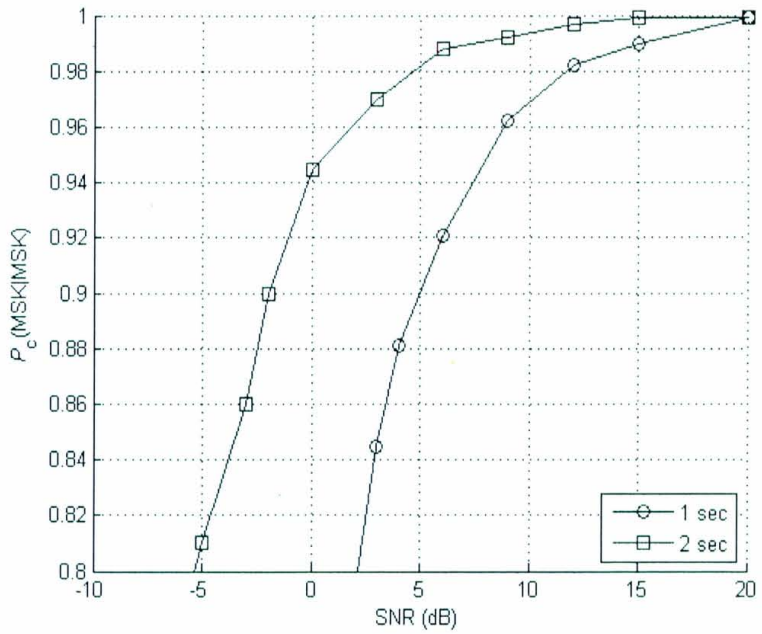

Figure 4.16: Classification performance versus SNR for MSK signals with different observation periods.

Figure 4.17 shows the MSK signal classification performance with one and two antennas using selection combining. One can observe that better performance is obtained when utilizing receive spatial diversity.

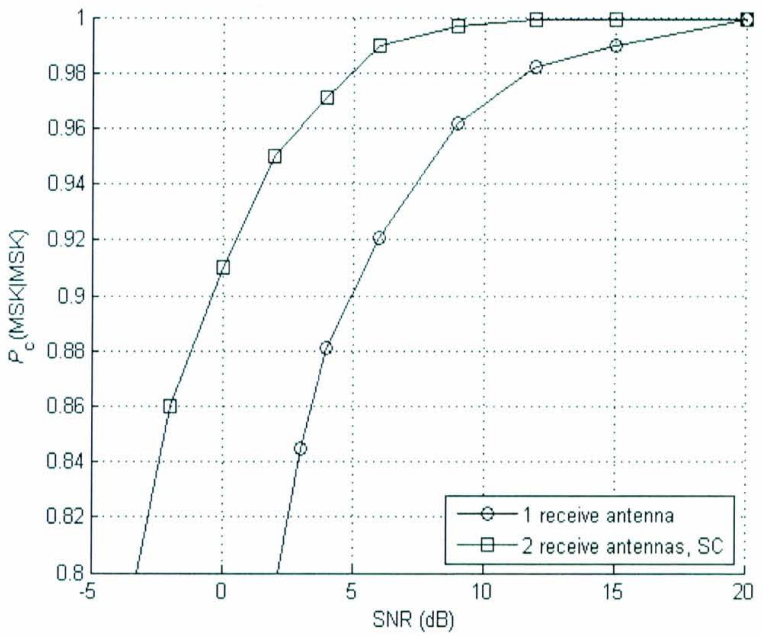

Figure 4.17: Classification performance versus SNR for MSK signals with one and two receive antennas.

4.5 Experimental results

4.5.1 Equipment description

4.5.1.1 Agilent N5182A RF vector signal generator (VSG) and signal studio software

The Agilent N5182A RF vector signal generator (Figure 4.18) combines state-of-the-art RF and digital signal processing to generate RF test signals. This is able to generate RF signals with a frequency range from 100 KHz to 6 GHz; the internal baseband generator has 100 MHz bandwidth and sample rate up to 125 MSa/s. The

Figure 4.18: Agilent N5182A RF VSG.

signal parameters such as carrier frequency, amplitude, modulation type, pulse shape, and symbol period can be adjusted. Users can also define the generated signal through the arbitrary waveform generator (ARB).

There are two approaches to generate signals. The first one is by using the multi-purpose mode of the instrument, where users can setup signal characteristics, such as the modulation type, symbol period, bandwidth, etc. The second approach is to use popular software programs, such as MATLAB, to generate signals and download such data files to the VSG memory. Then, the VSG is then able to generate RF signals based on the MATLAB signals.

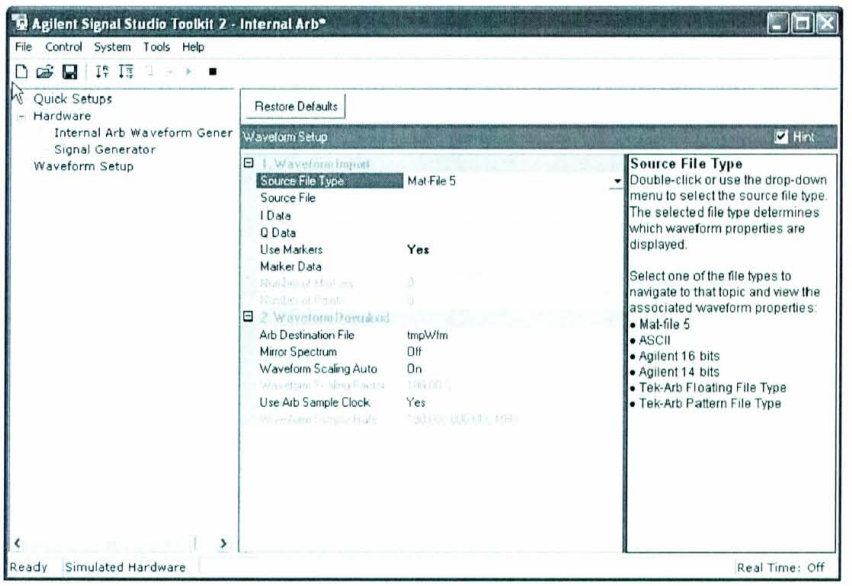

Figure 4.19: Agilent Signal Studio toolkit.

In our work, we use the second approach to generate experimental signals. The Agilent signal studio toolkit (Figure 4.19) is used to download MATLAB signals to the ARB, then using the digital-to-analog convertor (DAC) and up-conversion of the signal to the carrier frequency.

4.5.1.2 Keithley 2820 vector signal analyzer (VSA) and Agilent V2901A SignalMeister

The 2820 RF vector signal analyzer (Figure 4.20) is used to analyze received signals; this has a bandwidth up to 40 MHz, and accepts a carrier frequency from 400 MHz to 6 GHz. The received signal is down-converted to the intermediate frequency, bandlimited by a lowpass filter, and digitized by an analog-to-digital converter (ADC).

Figure 4.20: Keithley 2820 RF VSA.

There are three major functions of the VSA: spectrum analysis, vector signal analysis, and signal capture. In our work, we mainly apply the function of signal capture, which is able to capture a signal waveform with the duration up to 30 seconds. The captured signal data files are compatible with MATLAB. We upload these files to a personal computer, and apply our proposed algorithms for signal classification and tone frequency spacing estimation.

2800 VSA serves as the signal receiver, and the SignalMeister (Figure 4.21) SignalMeister receiver project (Figure 4.21) is used to operate the signal capture and record received signal data in the PC. Here, the block of 2800 VSA serves as the signal receiver, and General Purpose 1x Analysis is able to capture the received signal with a preset sweeping time and receive filter bandwidth.

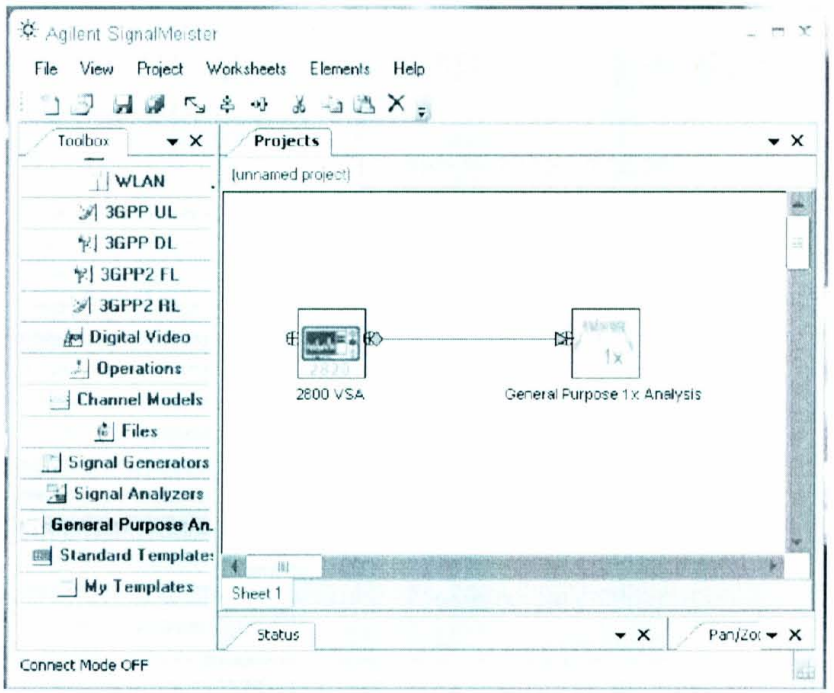

Figure 4.21: SignalMeister Software.

4.5.1.3 Hardware setup

In our experimental work, the equipments are connected as shown in Figure 4.22, which include an Agilent N5182A RF VSG, an 2820 RF VSA, and a personal computer. The transmitted signals are generated with the Agilent N5182A RF VSG, and received signals are captured with the 2820 RF VSA. The received signal is then uploaded to the personal computer, where we apply the proposed algorithms for classification and tone frequency spacing estimation.

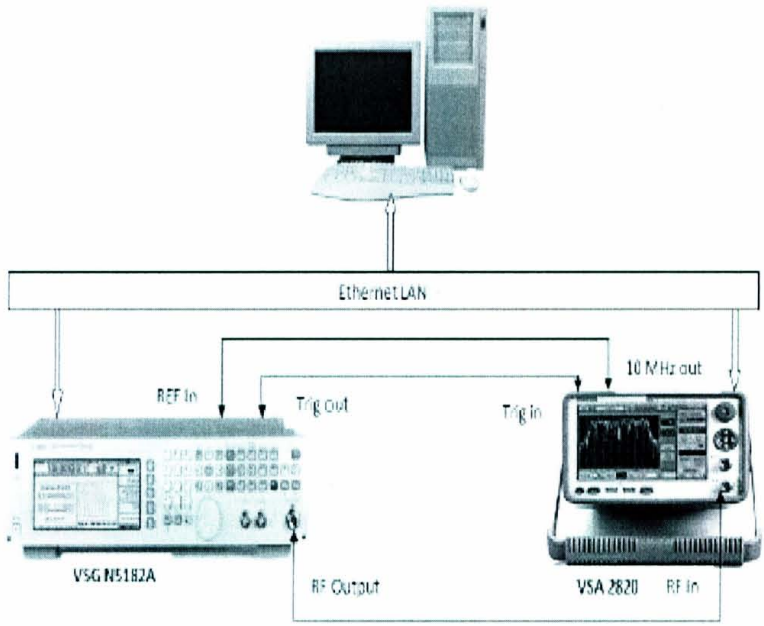

Figure 4.22: Experimental setup.

4.5.2 Experimental performance evaluation

We studied FSK and MSK classification and FSK tone frequency spacing algorithms experimentally. The parameters of FSK and MSK signals were set up as in Section 4.1. The performance of the algorithms in term of the probability of correct classification and estimation was calculated based on 300 Monte Carlo trials.

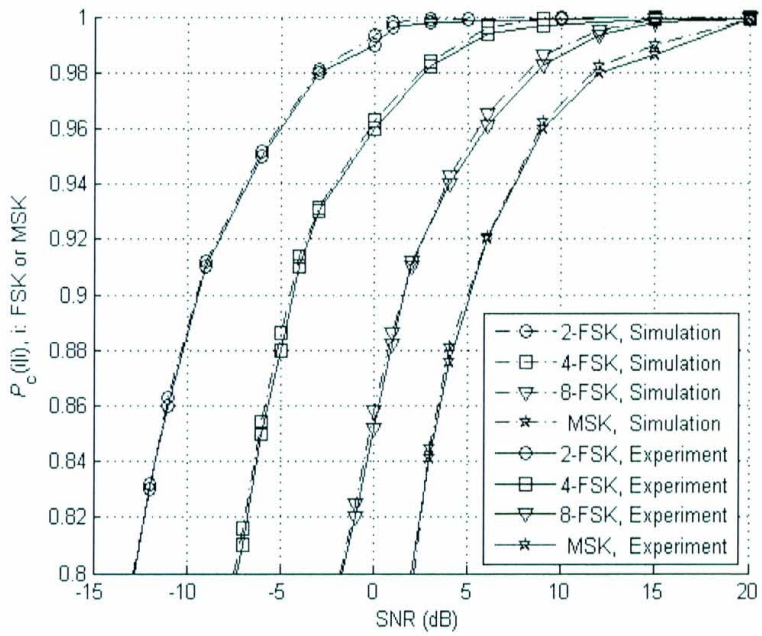

Figure 4.23: Simulation and experimental results for FSK and MSK signal classification.

Figure 4.23 presents the performance for FSK and MSK signal classification. As the figure shows, the simulation and experimental results are very close. This indicates that our proposed classification is practically efficient. Figure 4.24 shows the performance of the FSK signal tone frequency spacing estimation. As expected, the simulation and experimental results match.

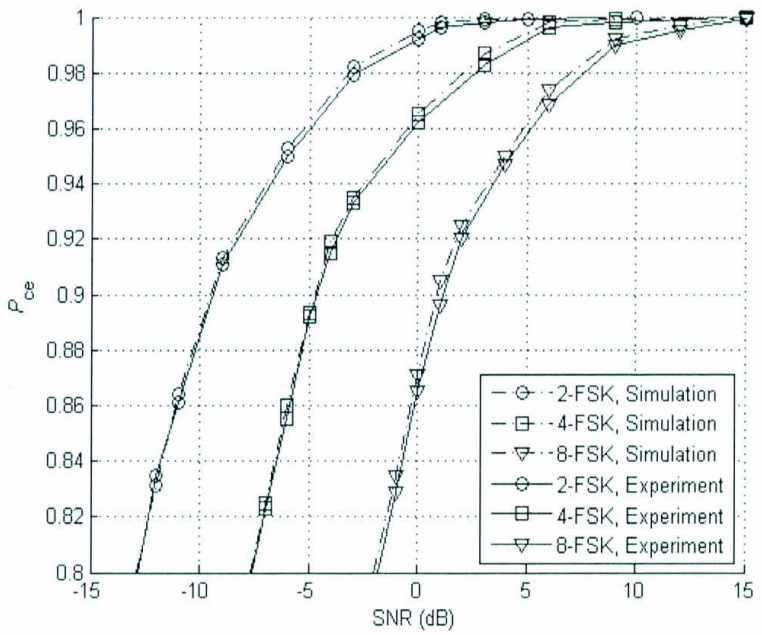

Figure 4.24: Simulation and experimental results for Ω-FSK signal tone frequency spacing estimation, $\Omega = 2, 4, 8$.

4.6 Summary

In this chapter, we presented the simulation results for three proposed algorithms: first-order cyclostationarity based FSK signal classification and tone frequency spacing estimation algorithm, second-order cyclostationarity based FSK signal symbol period estimation algorithm, and joint FSK and MSK signal classification algorithm. Moreover, the experimental results for signal classification and tone frequency spacing estimation were presented; these match the simulation results, which provides confidence in the design of the algorithms.

Chapter 5

Conclusions and future work

In this thesis, we proposed signal classification and parameter estimation algorithms for FSK and MSK signals affected by fading. The first-order cyclostationarity of FSK signals is investigated. Based on the first-order cyclostationary properties of FSK signals, we proposed a novel FSK signal classification and tone frequency spacing estimation algorithm. Then, we further exploited the second-order cyclostationarity of FSK signals, and proposed a symbol period estimation algorithm. Moreover, we studied the first- and second-order cyclostationarity of MSK signals, and proposed a joint FSK and MSK signal classification algorithm. Simulations were carried out to evaluate the performance of the proposed algorithms under diverse scenarios, such as different observation periods and SNRs. Simulation results showed that the proposed algorithms provide a reasonably good performance with short observation periods and low SNRs, yet affected by fading. The performance can be further improved with spatial diversity at the receive side. The proposed algorithms do not need pre-processing, such as timing and carrier recovery. The performance of the proposed algorithm is additionally investigated through laboratory experiments. The experimental signals are generated with the Agilent N5182 RF VSG, and captured with the Keithley 2820

VSA. Simulation and experimental results match, which proved the applicability of the proposed algorithms to real scenarios.

Future work

- In the first-order cyclostationarity-based algorithm, a preset cutoff value V_{co} was used to select candidate frequencies. Although we introduced an adaptive V_{co} to improve the algorithm performance, this is triggered only when less than two candidate frequencies are selected. A cutoff value which can be set adaptively under all conditions may further improve the performance of the algorithm.

- The second-order cyclostationarity of FSK signals is derived under the condition that $f_d T = l$, l integer. Deriving analytical expressions of the second-order cyclostationarity of any FSK signal represents an important aspect of future work. In the FSK symbol period estimation algorithm and joint FSK and MSK classification algorithm, we estimate the second-order cyclic moment of the received signal for a large enough delay. Such a large delay range increases the computational cost for real applications. Setting the delay range adaptively should be considered in future work.

- In the proposed work, we considered block fading. Other channel models need to be considered, as well, such as time-dispersive channels. This represents a direction of future work. Additionally, a single transmit antenna was considered. Multiple transmit antennas can be considered to improve the performance of the proposed algorithms; this also represents a direction of future investigation.

References

[1] O. A. Dobre, A. Abdi, Y. Bar-Ness, and W. Su, "A survey of automatic modulation classification techniques: classical approaches and new developments," *IET Commun.*, vol. 1, pp. 137-156, Apr. 2007.

[2] W. Gardner and C. Spooner, "Signal interception: performance advantages of cyclic-feature detectors," *IEEE Trans. Wireless Commun.*, vol. 40, pp. 149-159, Jan. 1992.

[3] J. L. Xu, W. Su, and M. C. Zhou, "Software-defined radio equipped with rapid modulation recognition," *IEEE Trans. Veh. Technol.*, vol. 59, pp. 1659-1667, May 2010.

[4] S. Haykin, "Cognitive radio: brain empowered wireless communication," *IEEE J. Sel. Areas Commun.*, vol. 23, pp. 201-220, Feb. 2005.

[5] FCC, "Report of the Spectrum Efficiency Working Group" ET Docket 02-135, Nov. 2002.

[6] F. Hameed, O. A. Dobre, and D. C. Popescu, "On the likelihood-based aproach to modulation classification," *IEEE Trans. Wireless Commun.*, vol. 8, pp. 5884-5892, Dec. 2009.

[7] S. Qinghua and Y. Karasawa, "Noncoherent maximum likelihood classification of quadrature amplitude modulaiton constellations: simplification, analysis, and extension," *IEEE Trans. Wireless Commun.*, vol. 10, pp. 1312-1322, Apr. 2011.

[8] A. Punchihewa, C. K. Bhargava, and C. Despins, "Blind estimation of OFDM parameters in cognitive radio networks," *IEEE Trans. Wireless Commun.*, vol. 10, pp. 733-738, Mar. 2011.

[9] A. Al-habashna, O. A. Dobre, R. Venkatesan, and D. C. Popescu, "Second-order cyclostationarity of mobile WiMAX and LTE OFDM signals and application to spectrum awareness in cognitive radio systems," *IEEE J. Selected Topics in Signal Process.*, vol. 6, pp. 26-42, Feb. 2012.

[10] B. Beidas and C. Weber, "Higher-order correlation-based approach to modulation classification of digitally frequency modulated signals," *IEEE J. Sel. Areas Commun.*, vol. 13, pp. 89-101, Jan. 1995.

[11] B. Beidas and C. Weber, "Asynchronous classification of MFSK signals using the higher order correlation domain," *IEEE Trans. Commun.*, vol. 46, pp. 480-493, Apr. 1998.

[12] K. Ho, W. Prokopiw, and Y. Chan, "Modulation identification of digital signals by the wavelet transform," *IEE Proc. Radar Sonar Navig.*, vol. 147, pp. 169-176, Aug. 2000.

[13] A. Rosti and V. Koivunen, "Classification of MFSK modulated signals using the mean of complex envelope," in *Proc. EUSIPCO*, Tampere, Finland, Sep. 2000, pp. 581-584.

[14] Z. Yu, Y. Shi, and W. Su, "M-ary Frequency shift keying signal classification based-on discrete Fourier transform," in *Proc. IEEE MILCOM*, USA, Oct. 2003, pp. 1167-1172.

[15] Y. Zhou, K. Qaraqe, E. Serpedin, and O. A. Dobre, "FSK-signal detection in cognitive radios using first-order cyclostationarity," in *Proc. IEEE ICT*, Qatar, Apr. 2010, pp. 110-115.

[16] Y. Zhou, K. Qaraqe, E. Serpedin, and O. A. Dobre, "AM-signal detection in cognitive radios using first-order cyclostationarity," in *Proc. IEEE ICASSP*, USA, Mar. 2010, pp. 3106-3109.

[17] O. A. Dobre, S. Rajan, and R. Inkol, "Joint signal detection and classification based on first order cyclostationarity for cognitive radios," *EURASIP J. Advances in Signal Process.*, doi:10.1155/2009/656719, July 2009.

[18] D. Grimaldi, S. Rapuano, and L. Vito, "An automatic digital modulation classifier for measurement on telecommunication networks," *IEEE Trans. Instrum. and Meas.*, vol. 56, pp. 1711-1720, Oct. 2007.

[19] L. Vito, S. Rapuano, and M. Villanacci, "Prototype of an automatic digital modulation classifier embedded in a real-time spectrum analyzer," *IEEE Trans. Instrum. and Meas.*, vol. 59, pp. 2639-2651. Oct. 2010.

[20] A. El-Mahdy and N. Namazi, "Classification of multiple M-ary frequency shift keying signals over a Rayleigh fading channel," *IEEE Trans. Commun.*, vol. 50, pp. 967-974, Jun. 2002.

[21] J. Tan, A. Sha'ameri, and Y. Chee, "Signal analysis and classification of digital communication signal using time-frequency analysis techniques in the multipath

fading environment," in *Proc. ISSPA*, Kuala Lumpur, Malaysia, May. 2010, pp. 678-681.

[22] K. C. Ho, W. Prokopiw, and Y. T. Chan, "Modulation identification of digital signals by the wavelet transform," *IEE Proceedings on Radar, Sonar and Navigation,* vol.147, pp. 169-176, Aug. 2001.

[23] Y. T. Chan, J. W. Plews, K. C. Ho, "Symbol rate estimation by the wavelet transform," in *Proc. ISCAS '97*, Hong Kong, Jun. 1997, pp. 177-180.

[24] J. Xu, F. P. Wang, and Z. J. Wang, "The improvement of symbol rate estimation by the wavelet transform," in *Proc. International Conference on Communications, Circuits and Systems,* pp. 100-103, May 2005.

[25] Y. Pao and D. J. Sobajic, "Combined use of unsupervised and supervised learning for dynamic security assesment," *IEEE Trans. Power Systems*, vol. 7, pp. 878-884, May 1992.

[26] O. Andrisano and M. Chiani, "The first Nyquist criterion applied to coherent receiver design for generalized MSK signals," *IEEE Trans. Commun.*, vol. 42, pp. 449-457, 1994.

[27] J. Anderson, T. Aulin, and C. Sundberg, *Digital Phase Modulation.* New York: Plenum, 1986.

[28] Y. Ramakonar, D. Habibi, and A. Bouzerdoum, "Automatic recognition of digitally modulated communications signals," in *Proc. ISSPA '99*, Brisbane, Australia, vol. 2, pp. 753-756, Aug. 1999.

[29] A. Kubankova, D. Kubanek, and J. Prinosil, "Digital modulation classification based on characteristic features and GentleBoost algorithm," in *Proc. International Conference on Telecommun. and Signal Process.*, pp. 448-451, Aug. 2011.

[30] E. Rebeiz and D. Cabric, "Low complexity feature-based modulation classifier and its non-asymptotic analysis," in *Proc. Globecom 2011*, pp. 1-5, Houston, Texas, USA, Dec. 2011.

[31] C. Schreyogg, K. Kittel, U. Kressel, and J. Reichert, "Robust classification of modulation types using spectral features applied to HMM," in *Proc. MILCOM 97*, vol. 3, pp. 1377-1381, Nov. 1997.

[32] A. Dandawate and G. Giannakis, "Statistical tests for presence of cyclostationarity," *IEEE Trans. Signal Process.*, vol. 42, pp. 2355-2369, Sep. 1994.

[33] R. Burden and J. Faires, *Numerical Analysis*, Boston, USA: Brooks Cole, 2004.